QUANTIFYING THE INTERACTION BETWEEN CLIMATE AND LANDSCAPE ON WATER RESOURCES

by

Andrew Gelderloos

A thesis submitted to the faculty of
The University of Utah
in partial fulfillment of the requirements for the degree of

Master of Science

in

Geology

Department of Geology and Geophysics

The University of Utah

May 2018

The University of Utah Graduate School

STATEMENT OF THESIS APPROVAL

The thesis of **Andrew Gelderloos**

has been approved by the following supervisory committee members:

Paul D. Brooks	, Chair	**1/9/18** Date Approved
Douglas Kip Solomon	, Member	**1/9/18** Date Approved
Courtenay Strong	, Member	**1/17/18** Date Approved
William Anderegg	, Member	**1/16/18** Date Approved

and by **Thure E. Cerling** , Chair/Dean of

the Department/College/School of **Geology and Geophysics**

and by David B. Kieda, Dean of The Graduate School.

ABSTRACT

Water resources face increasing stress from climate change that may not result in uniform vulnerability to hydrologic response across all watersheds. I compare over 100 years of historical hydrologic data from seven seasonally snow-dominated watersheds near Salt Lake City, Utah to identify how watershed landscapes interact with climate variability to control hydrologic partitioning. Mean annual precipitation (790 mm - 1290 mm) and temperature (3.3°C - 6.9°C) differ primarily as a function of watershed elevation. Mean annual streamflow, normalized by watershed area (150 mm to 820 mm), differs primarily as a function of mean precipitation. Precipitation and temperature exhibit similar interannual variability. However, due to the unique landscape characteristics of the watersheds, streamflow values exhibit large differences in interannual variability between the watersheds. Interannual variability in precipitation explains between 46%-73% of the annual variability in streamflow. Surprisingly, the remaining variability does not correlate to annual or seasonal temperature. Instead, interannual variability in subsurface storage and snowmelt processes further reduce the uncertainty in annual streamflow. Together, precipitation, storage, and snowmelt explain nearly all (96%-98%) of the annual variability in streamflow. Storage accounts for a legacy effect of past climate on streamflow that varies between watersheds based on subsurface characteristics. The rate of snowmelt affects the snowpack's infiltration efficiency and is primarily controlled by solar radiation, varying between watersheds

based on hillslope shading characteristics. These controls on hydrologic partitioning indicate that subsurface and topographic characteristics control the differential sensitivity of watersheds to changes in climate.

TABLE OF CONTENTS

LIST OF TABLES

Tables

LIST OF FIGURES

Figures

CHAPTER 1

INTRODUCTION

1.1 Water Challenges in Utah

Water supply variability causes tremendous disruption to society. Threats of flooding and drought lurk at opposite ends of the spectrum of water availability. While evidence of the tension between people and water extends back many millennia to the beginning of civilizations (Hassan, 2010; Juuti et al., 2007), the recent history in the state of Utah provides ample illustration of this delicate balance. For example, drought in 1977 led to widespread economic losses ranging from losses in crops, livestock, and farmland to a 50% revenue reduction in an otherwise booming ski industry (Hughes et al., 1978). Merely 6 years later, flooding in 1983 led to overflowing rivers being channeled down streets in Salt Lake City and statewide damages in excess of $250 million (Anderson et al., 1984). Utah has used the lessons learned from these disasters to better prepare for and prevent the negative outcomes of similar climate events in the future (Bowles et al., 1980; Wieczorek et al., 1989). However, Utah, as well as every other community influenced by water availability in the world, faces challenges from climate change that may make conventional assumptions learned from past hydrologic events and trends obsolete (N. S. Christensen et al., 2004; Maurer & Duffy, 2005; Milly et al., 2008). Rather than designing water management strategies adapted for the range of historical observations,

hydrologic systems must be understood and managed as environments with differential responses to dynamic supplies and demands.

Approximately one sixth of the world's population relies on mountain watersheds for their water supply (Barnett et al., 2005). In many of these areas, including Utah and the rest of the Western United States, population growth increases the demands on these vital water resources (Arnell, 1999; Utah Foundation, 2014; Yigzaw & Hossain, 2016). More people will not only require more water for drinking, but more importantly will require more food (grown using water), more energy (produced using hydropower and other water-intensive processes), and more industrial manufacturing, all while having a similar reliance on ecosystem services (Burnham et al., 2016; Gleick, 2003). At the same time that a growing population increases the demand on water resources, it will also increase the area of built infrastructure that must be protected from extreme flooding events (Hollis, 1975).

Climate change further exacerbates water resource challenges. Human-induced climate change is projected to cause an increase in extreme precipitation events that are expected to speed up the hydrologic cycle (Hirabayashi et al., 2013; Oki & Kanae, 2006). Numerous studies indicate reductions in streamflow throughout the Western United States will occur as a result of projected climate changes due to the increased evapotranspiration from warmer temperatures and reductions in mountain snow pack (Barnett et al., 2005; Barnett & Pierce, 2008; N. S. Christensen et al., 2004). Advances in climate modelling allow for ensemble models to run many iterations to project probabilistic future climate scenarios (Meehl et al., 2007; Milly et al., 2008). The models provide an increasing ability to quantify how vulnerable different regions are to changes

in temperature and precipitation under current and future natural and anthropogenic emissions scenarios (Fowler et al., 2007; Maraun et al., 2010).

1.2 The Role of the Watershed

Regional and downscaled models improve the precision and accuracy of climate projections in local regions (Vrac et al., 2007). It is at these local scales that water managers make decisions that will affect stakeholders that can include drinking water users, agriculture, and ecosystem services. Of course, water planners must provide projections of future water availability, not simply projections of temperature and precipitation (Barnett et al., 2005; Gosling & Arnell, 2016). Therefore, the relationship between climate and the hydrologic response within individual watersheds will facilitate the risk posed by future climate change to societies.

Inputs to headwater mountain watersheds are generally straightforward; they can be measured on the surface of a delineated catchment area through point-source measuring devices and interpolated over vast areas (Hornberger et al., 2014). Subsurface inputs are generally minimal in mountainous headwater catchments (Hornberger et al., 2014). Therefore, precipitation constitutes the major addition of water into the catchment. Precipitation can occur as either rain or snow, with snow making up between 50% and 80% of the mean annual precipitation in mountain watersheds in Northern Utah, depending primarily on watershed elevation (NRCS National Water and Climate Center, 2017).

Hydrologic partitioning is a term used to describe the processes that divide water inputs into different outputs. Water availability, both to human and to atmospheric

demands, can only be calculated through an understanding of the partitioning of inputs, typically precipitation, through a watershed.

Water exits the catchment through streamflow, evapotranspiration, groundwater throughflow, and man-made diversions. Due to the accessibility of streamflow, most human diversions in mountain catchments come from surface water (Hely et al., 1971). For the purpose of this study, man-made diversions are aggregated into streamflow totals. The streamflow, water not lost to atmospheric demands, typically constitutes the amount of water available for human use or management. Groundwater throughflow is one of the primary contributors to the valley aquifer, even though it is not a major source of catchment output (Hely et al., 1971; Manning & Solomon, 2005). Most water exits the watershed via streamflow or evapotranspiration.

Total evapotranspiration is the combination of all water lost to atmospheric demands, including evaporation, sublimation, and transpiration. Evaporation, by definition, occurs at a wet surface where liquid moisture vaporizes. This may happen directly at the surface or in the shallow subsurface where water vaporizes within the soil matrix before diffusing into the atmosphere (Penman, 1948; Xiao et al., 2011). Similar processes, in addition to sublimation, may occur within a snowpack (DeWalle & Rango, 2008).

Precipitation that infiltrates into the subsurface is available to transpiration from vegetation. Plants draw moisture from the soil through their roots, which can extend tens of meters into the subsurface (Canadell et al., 1996). Annual transpiration typically begins as the amount of solar radiation increases during the spring and continues until solar radiation decreases in the fall or the soil moisture the vegetation draws from

depletes past the permanent wilting point. All evapotranspiration from saturated soil conditions is limited by available energy, typically from solar radiation and ambient temperature, at a rate referred to as potential evapotranspiration (Hornberger et al., 2014). Actual evapotranspiration may be less than potential evapotranspiration when the ground is not completely saturated or when plants limit transpiration by closing their stomata (L. Christensen et al., 2008; Hornberger et al., 2014; Penman, 1948).

Streamflow, in contrast to evapotranspiration, generally consists of excess water unable to be retained in the watershed's surface and subsurface reservoirs, flowing downgradient due to gravity until it exits the catchment. Streamflow consists of a quick and a slow response to mobile water added to the watershed from storms or snowmelt (Hornberger et al., 2014). Both types of streamflow generation typically consist of water that has been stored in the watershed subsurface for more than a year (Brooks et al., 2015; Godsey et al., 2009). A quick response occurs when new water enters preferential flowpaths in the subsurface of the watershed and displaces stored water, forcing it downgradient and into stream channels (Bazemore et al., 1994; Frisbee et al., 2012; Sklash & Farvolden, 1979; Williams & Melack, 1991). In snow-dominated watersheds, the majority of quick flow is a response to snowmelt. Initial snowmelt during the early spring saturates the subsurface and increases subsurface hydrologic connectivity (Croft, 1944b; McNamara et al., 2005). Snowmelt pulses during the late spring and early summer occur when hydrologic connectivity in the subsurface is typically the greatest, allowing the meltwater pulse to directly influence the level of streamflow (Croft, 1944b). In contrast, late summer storm events that occur when there is low soil moisture content and high vegetation demand may not generate a quick flow response when the storm

water fails to adequately saturate the subsurface (Croft & Monninger, 1953).

A slow streamflow response occurs as groundwater slowly flows downgradient through the porous subsurface of the watershed until reaching a stream channel. Unlike quick response that can subside minutes to days after an event, the slow response can be sustained for months or years after an event and, therefore, is often an accumulation of many years of hydrologic events (McNamara et al., 2011). Slow flow is typically governed by Darcy's Law for groundwater flow, which states that the discharge from a porous media relates to the pressure gradient and hydraulic conductivity of the aquifer (Hornberger et al., 2014). Therefore, slow flow combines climatological supply and demand with physical watershed characteristics. The relative amount of water stored in the subsurface, which is conducive to past precipitation supply and atmospheric demand, in combination with topography controls the pressure gradient in a watershed. Hydraulic conductivity is a property of the permeability of the porous aquifer.

Partitioning of precipitation to evapotranspiration and streamflow determines the amount of available water resources. Climate conditions influence partitioning through the supply and timing of precipitation and through controls on the energy balance. In the absence of precipitation changes, current models suggest warming temperature trends will directly correlate to streamflow and water availability through increased losses to atmospheric demands. This simplifies watershed partitioning, allowing for predictions of watershed vulnerability to climate change without necessitating decades-long research to understand every aspect of catchment partitioning. However, these assumptions may make too many simplifications. Watershed characteristics influence partitioning through controls on the routing and residence time of water through the catchment. If these

controls on partitioning are significant, watershed vulnerability to climate change may vary between catchments in similar climate regimes and cause inaccurate projections of future water availability to be made.

In this thesis, I present a review of the expected hydrologic response to climate change in snow-dominated mountain headwater catchments in the Intermountain West of the United States. Using an extensive historic dataset, I examine whether simple climate metrics, including precipitation and temperature, can explain the variable partitioning that exists in catchments that experience similar climate forcing. Lack of correlation between temperature and variable partitioning suggests that water availability projections should not be entirely temperature-dependent. Instead, the importance of variable interannual subsurface storage and snowmelt provides guidance to identifying the watershed characteristics that significantly control partitioning.

CHAPTER 2

PRESENT STUDY

2.1 Introduction

Societies and ecosystems rely on adequate water resources for current and future sustainability. However, water resources face increasing demands from population growth (Arnell, 2004; Vörösmarty et al., 2000) and increasing stress from climate changes that affect the supply of water, through precipitation, and the evaporative demands on water in watersheds (Barnett et al., 2005; Bates et al., 2008; Trenberth, 2011). As climate conditions change, water management decisions must be made to anticipate and mitigate the impacts of future water availability and extreme hydrologic events (Bardsley et al., 2013; Barnett & Pierce, 2008; Gleick, 1989). It has been recognized, however, that future decisions cannot be made under the assumption of long-term statistical stationarity in watersheds (Milly et al., 2008). Instead, predicting the amount of water available for increasing demands presents a challenge that must be solved through a physical understanding of how changing climate conditions will manifest in watershed hydrologic systems (Kirchner, 2006).

Numerous studies have identified the expected response of streamflow to climate change at both global (Arnell, 1999; Milly et al., 2005; Nijssen et al., 2001) and continental climate scales (Cayan et al., 2008; Gosling & Arnell, 2016). However,

regional and individual watersheds exhibit differential responses to climate at scales relevant for catchment management decisions (Chase et al., 2016; Pourmokhtarian et al., 2017). Watershed-specific characteristics affect the partitioning of precipitation to streamflow (Troch et al., 2013; Zapata-Rios et al., 2015). Some approaches attempt to account for variable partitioning through differences in catchment elevation (Dingman, 1981; Tennant et al., 2015), geology and soils (Mayer & Naman, 2011; Wolock & McCabe, 1999), and vegetation (Bosch & Hewlett, 1982; Zhao et al., 2010). However, transferable metrics based on intrabasin watershed processes that link climate forcing and landscape partitioning with streamflow remain elusive (Beven, 2006; Brooks et al., 2015).

Snow-dominated mountain watersheds are especially important, providing water for nearly 1/6 of the world's population and most of the population in the western United States (Bales et al., 2006; Barnett et al., 2005). In the western United States, climate change has been linked to reduction in April 1 snow water equivalent (N. S. Christensen et al., 2004; Hamlet et al., 2005; Mote, 2006), more winter precipitation falling as rain rather than snow (Barnett et al., 2008; Knowles et al., 2006), changing snowmelt rates (Barnett et al., 2005; Harpold et al., 2012), and the timing of the spring snowmelt pulse in streamflow (Barnett et al., 2008; Cayan et al., 2001; Clow, 2009; Stewart et al., 2005). The precise impact of climate forcing on watershed snowpacks depends on landscape characteristics, such as slope aspect and vegetation cover, which control the surface energy balance (Croft, 1944b; Hinckley et al., 2014; Zapata-Rios et al., 2015). Although we currently lack the ability to adequately model snowpack changes within ungauged basins (Barnhart et al., 2016; Biederman et al., 2015), it is clear that significantly

different hydrologic responses should be expected from different controlling factors (Bales et al., 2006; Foster et al., 2016).

Salt Lake City in northern Utah relies on water that primarily originates in continental mountain watersheds. Over 60% of the water resources for the approximately one million people who live in the semiarid valley originates as surface water in the Wasatch Mountains and nearly all of the remaining 40% consists of groundwater recharged from mountain precipitation or comes from surface water from other nearby mountains (Bardsley et al., 2013; Hely et al., 1971). Water resources in the region will face increasing demands as the population of Salt Lake County is expected to increase by 60% within the next 35 years (Utah Foundation, 2014). Current hydrologic models for Salt Lake City area watersheds indicate future streamflow will decrease by 1.8% - 6.2% for every 0.56°C of warming based on increased evapotranspiration losses from a lengthening of the growing season (Bardsley et al., 2013). The combined stress of the increase in demands and the decrease in supply necessitates a rigorous, physically-based understanding of how regional-scale climate conditions will affect localized water resources within different landscapes.

Growing reliance on mountain catchments in the Intermountain West leads to an increasing demand for accurate models of water availability at local watershed scales. However, the hydrologic cycle within a catchment has the potential to be affected by many different landscape features that would alternately cause watersheds with similar climate forcing to experience different responses in water resources. Therefore, I ask the question: How do landscapes differentially interact with climate to affect streamflow? Building on the foundation from this question, I further ask: Can I identify simple and

transferable metrics that can incorporate the influence of landscapes to more accurately predict streamflow?

2.2 Site Description

2.2.1 Location and Landscape

The study area is located in the intermountain region of the Western United States; specifically, in the Wasatch Mountain Range east of Salt Lake City, Utah (Figure 2.1). The Wasatch Mountains are the western-most range of the Rocky Mountains at a latitude of approximately 41° N and border the Basin and Range physiographic province on their western edge. Over the past 10-12 million years, the range was uplifted by a normal fault on the eastern edge of the Salt Lake Valley, exposing rock layers ranging from Middle Proterozoic to Tertiary in age (Ehlers et al., 2003; Granger, 1953; Nichols & Bryant, 1990). This uplift raised the mountains, which now peak at 3500 meters above sea level, over 2200 meters above the valley floor at 1300 meters above sea level.

The seven watersheds included in this study have creeks that flow from their headwaters in the Wasatch Mountains into the Salt Lake Valley where they connect with the Jordan River before reaching the Great Salt Lake. These creeks all flow generally from east to west through canyons that are oriented towards the west. From north to south, the creeks are: City Creek (CC), Red Butte Creek (RB), Emigration Creek (EC), Parleys Creek (PC), Mill Creek (MC), Big Cottonwood Creek (BC), and Little Cottonwood Creek (LC). Daily streamflow observations from the Salt Lake City Department of Public Utilities date back to 1902 in CC, EC, PC, MC, and BC; 1911 in LC; and from the USGS date back to 1961 in RB, with monthly observations in RB from

1942 – 1960.

Stream gauges on all of the creeks are located near the mouths of the canyons at relatively similar elevations, ranging from 1380 m to 1650 m with a mean of 1510 m. The highest average watershed elevation occurs at 2700 m in the southernmost watershed, LC, and average elevation lowers progressively to the north until reaching 1960 m in RB, where average elevation begins to increase toward the north (Table 2.1). Maximum elevations within individual watersheds generally occur on the northern or southern, rather than the western, margins of the watersheds. Similar to average watershed elevation, the highest maximum elevation occurs at 3500 m in the southernmost watershed, LC, and decreases to 2530 m in RB before increasing again to the north.

The northern watersheds: CC, RB, EC, PC, and MC are underlain almost entirely by Upper Cretaceous – Cambrian sedimentary carbonates and clastic layers, consisting primarily of sandstone and limestone (Granger, 1953; Nichols & Bryant, 1990). The Parleys Canyon Syncline runs through PC with a fold axis that trends from SW to NE and plunges toward the NE and dominates the geologic structure of the northern watersheds (Nichols & Bryant, 1990). As a result, sedimentary layers on the flanks of the syncline in CC, RB, southern PC, and MC are tilted to a nearly vertical orientation in some places (Ehleringer et al., 1992; Nichols & Bryant, 1990). Late to Middle Proterozoic shale, siltstone, and quartzite dominate the western portion of BC while Oligocene quartz monzonite dominates the western portion of LC (Granger, 1953; Nichols & Bryant, 1990). Eastern portions of BC and LC contain sedimentary layers similar to the northern watershed, ranging from Middle Proterozoic to Triassic (Granger, 1953; Nichols & Bryant, 1990). The eastern portions of BC and LC also include Oligocene diorite and

monzonite plutons (Nichols & Bryant, 1990). Extensive glacial activity during the last glacial maximum (approximately 10 – 50 ka) in BC and LC, and to a more limited degree in CC and MC, reshaped the landscape by scouring soils from the surface and, in some cases, redistributing this soil in moraines further down the canyon (Atwood, 1909; Biek et al., 2010).

Differences in elevation and the underlying geologic structure control topographic characteristics, causing differences in slope aspect and topographic shading. Similarly, the extent of glacial processes and the characteristics of the underlying geologic structure control the hydrologic properties of the subsurface.

The distribution of vegetation in the seven watersheds reflects elevational gradients, presence of a well-developed soil profile, as well as energy and water availability. Ecosystems range from low elevation desert scrub to high elevation alpine meadow (Ehleringer, 1988). Densely vegetated riparian communities supporting stands of cottonwood, boxelder, and birch trees exist adjacent to the creeks and their tributaries (Ehleringer et al., 1992). Other major ecosystem types include: grasslands, typically found at low elevation, south-facing slopes; scrub oak and scrub maple, typically found throughout the low- to mid- elevations; and aspen/conifer forests, typically found at higher-elevation, north-facing slopes (Ehleringer, 1988; Ehleringer et al., 1992). Minimally-vegetated rock outcroppings and talus slopes exist throughout all watersheds, but are most common in BC and LC (Table 2.1).

2.2.2 Climate

The Intermountain West climate is generally semiarid with tremendous precipitation and temperature variability due to a large range of elevation and varying topography ("Western Water Assessment," 2017). In general, the climate becomes cooler and wetter with increasing elevation. Weather patterns typically move from west to east, losing moisture over the Maritime mountain ranges near the West coast before reaching the Intermountain West (Wise, 2012). As a result, this region receives less precipitation than the Maritime ranges but more than the Continental ranges further east (Armstrong & Armstrong, 1987).

Seasonally, most precipitation (50% - 80%) occurs during the winter as snowfall rather than during the summer as rain (NRCS National Water and Climate Center, 2017; "Western Water Assessment," 2017; Wise, 2012). At a latitude of 41°N, the angle of the sun in the sky varies drastically throughout the year, causing large fluctuations in the energy input to the environment. Based on elevation and topography, seasonal snowpack typically begins to accumulate in October or November, peaks during March or April, and finishes ablating between May and July (NRCS National Water and Climate Center, 2017).

The climate observed in the Salt Lake Valley (elevation 1300 m) is representative of a semiarid environment. The mean monthly temperature in Salt Lake City ranges from -1.4°C in January to 25.9°C in July. Mean annual precipitation is 410 mm, with a monthly peak in April of 50 mm and a minimum in July of 15 mm (Western Regional Climate Center, 2017). In contrast, the Wasatch Mountains east of the valley generate more rainfall and have lower temperatures due to orographic uplift and elevational lapse

rates (Hely et al., 1971). For example, at an elevation of 2700 m, the Alta climate station in Little Cottonwood Canyon ranges from -5.8°C in January to 16.9°C in July while averaging 1400 mm of annual precipitation (Western Regional Climate Center, 2017). In addition to the climate variability caused by elevational gradients, climate can also be affected by the orientation of individual watersheds to incoming storm systems and topographic complexities affecting small-scale atmospheric interactions (Schultz et al., 2002; Steenburgh & Alcott, 2008).

Future climate projections indicate a warming trend throughout the study area (Bardsley et al., 2013; Scalzitti et al., 2016). Future precipitation projects generally indicate that the study area is in a transitional zone of no future trends between decreasing precipitation trends in the Southwest US and increasing precipitation trends in the Northwest US (Bardsley et al., 2013). However, extreme precipitation events are expected to increase in frequency (Garfin et al., 2013). Historic snowpack observations and models of future snowpack conditions indicate a likely decline in snowpack and an earlier onset of spring snowmelt throughout the Western US (Clow, 2009; Harpold et al., 2012; Stewart et al., 2004). Similarly, projections indicate a shift in the timing of snow cover, as the magnitude of snowpack extending into late-spring and summer is expected to decline (Garfin et al., 2013)

2.3 Methods

2.3.1 Approach

This thesis organizes over 100 years of historical hydrologic data from seven watersheds into 75 metrics that could plausibly be used to predict annual streamflow. An

evaluation of streamflow and these 75 metrics compares the hydrology of the seven watersheds as well as the historical distribution and trends of the datasets. Correlations between streamflow and predictive metrics provide insight to the factors controlling the amount of streamflow and the partitioning of water within a catchment. The approach for this is described in the following sections and consists of 1) development of hydrologic metrics; 2) analysis of hydrologic metrics; 3) prediction of streamflow; and 4) consideration of vegetation controls on stored water.

2.3.2 Development of Hydrologic Metrics

Precipitation, temperature, and relative humidity data originate from Parameter-elevation Regression on Independent Slopes Model (PRISM) climate records (PRISM Climate Group, 2015). PRISM calculates historical precipitation and temperature datasets interpolated using climate-elevation regressions and historic climate station data (Daly et al., 2008). Coverage of monthly precipitation (in mm), temperature (in °C), and dew point temperature (in °C) is available at 4km grid size resolution across all of the watersheds for water years 1896 – 2014. Watersheds consist of a combination of 6 – 19 partial or whole grid cells, based on the size and orientation of the watershed.

For precipitation in each watershed, the data value of each 4km grid is weighted by the fractional area of the given grid that is contained within the given watershed. The summation of all watershed grid values weighted by the fractional area results in the total monthly value for the entire watershed. By definition, this value remains in the one-dimensional unit of mm and is therefore comparable between watersheds, unlike volume, which is dependent on watershed area.

For temperature and dew point temperature in each watershed, the data value of each 4km grid is weighted by the fractional area of the given watershed that is contained within the given grid. The summation of all watershed grid values weighted by the fractional area results in the mean monthly value for the entire watershed.

Mean temperature and dew point temperature convert to relative humidity using the August-Roche-Magnus approximation (Alduchov & Eskridge, 1996; Lawrence, 2005):

$$Relative\ Humidity = 100 * \frac{e^{\frac{aT_d}{b+T_d}}}{e^{\frac{aT}{b+T}}} \quad (2.1)$$

where a and b are empirical constants equal to 17.625 and 243.04, respectively, T_d is dew point temperature in °C, and T is mean temperature in °C.

Annual and seasonal metrics are created for precipitation, temperature, and relative humidity. Seasons include fall (September – November), winter (December – February), spring (March – May), and summer (June – August). Annual metrics are compiled using the water year, which begins October 1 and ends September 30. The summation of precipitation over all included months results in the annual or seasonal value. The mean temperature or relative humidity of all included months results in the corresponding annual or seasonal value.

Daily streamflow discharge data, provided by Salt Lake Public Utilities, is available for CC, EC, PC, MC, and BC during water years 1902 – 2014 and in LC during water years 1911 – 2014. Streamflow discharge data, provided by the USGS National

Streamflow Information Program, are available for RB at a monthly time step during water years 1942-1961 and at a daily time step during water years 1962 – 2014. For each watershed, streamflow discharge divided by watershed area results in normalized streamflow values in one-dimensional mm units comparable to precipitation values. Total annual streamflow aggregates daily or monthly streamflow values over each water year (October – September).

Relative levels of each watershed's subsurface stored water manifest in winter baseflow in seasonally snow-dominated watersheds (Peralta-Tapia et al., 2015; Winter, 2007). Winter baseflow is calculated as the mean streamflow during December and January. During this time, incoming precipitation has a minimal contribution to subsurface storage or streamflow because it remains above the surface in the snowpack. Additionally, during this time, evapotranspiration does not affect the level of subsurface storage because vegetation is largely dead or dormant (Weaver & Mogensen, 1919; Winter et al., 1998). Therefore, winter baseflow represents the relative level of subsurface storage in each watershed (Wittenberg & Sivapalan, 1999).

Snowmelt causes a distinct increase in daily streamflow from winter baseflow before returning back to baseflow conditions after the snowpack has melted. The onset of snowmelt is objectively identified in the hydrograph as the day that streamflow exceeds three standard deviations of mean December and January streamflow. To ensure that this increase indicates the beginning of seasonal melt and not a short-term climatic event, streamflow must remain above three standard deviations of baseflow for at least three consecutive days. Therefore, to identify the start of snowmelt using streamflow observations, the following equation is used for each water year:

$$Q_d \& Q_{d+1} \& Q_{d+2} > 3 * \left(Standard\ Deviation(Q_b)\right) \quad (2.2)$$

where Q_d is daily streamflow and Q_b is daily streamflow during December and January. Snowmelt ends when streamflow returns to baseflow conditions from the previous winter. Specifically, this is calculated as the first day after the day of peak streamflow where daily streamflow is within three standard deviations of the previous mean December and January streamflow. To ensure this day is not an outlier, streamflow must remain within three standard deviations of baseflow for at least three consecutive days. Using these objective streamflow metrics, snowmelt rate is calculated:

$$Melt\ Rate = \frac{Q_{melt}}{melt\ duration} \quad (2.3)$$

where melt rate is calculated in mm/day, melt duration is the total number of days between the start and end of snowmelt, and Q_{melt} is the summation of daily streamflow, in mm, during the snowmelt duration.

Water yield, a dimensionless value, represents the fraction of annual precipitation partitioned to annual streamflow. Water yield is calculated as

$$Water\ Yield = \frac{Annual\ Streamflow}{Annual\ Precipitation}. \quad (2.4)$$

Water yield is correlated to landscape characteristics including elevation, aspect, slope steepness, and land cover using linear regression analysis. To test whether correlations

are dependent on any single watershed, this regression analysis is repeated while omitting each watershed.

Precipitation that is not partitioned to streamflow is often categorized as evapotranspiration (ET) because losses to groundwater tend to be small (Hornberger et al., 2014). Therefore, ET is calculated as

$$ET = P - Q. \tag{2.5}$$

Because ET typically represents a large outflow of precipitation from a watershed, vegetation, a dominant controller of ET, presumably plays an important role in watershed partitioning (Hornberger et al., 2014). However, a portion of precipitation is not available to vegetation, represented by a stormflow pulse that discharges from the watershed during storm or snowmelt events (Brooks et al., 2011). Stormflow (S) is separated from baseflow (U) using the recursive filter

$$U_k = aU_{k-1} + \frac{1-a}{2}(Q_k + Q_{k-1}), \tag{2.6}$$

$$U_k \leq Q_k$$

$$S_k = Q_k - U_k$$

where the filter parameter, a, is set to 0.925 (Lyne & Hollick, 1979; Voepel et al., 2011). The total amount of annual precipitation available to atmospheric demands, or wetting (W), is calculated as

$$W = P - S. \quad (2.7)$$

Identified by Horton (1933) and developed by Troch (2009), the Horton Index is a dimensionless watershed metric that represents the water use efficiency of atmospheric demands on plant-available water (Troch et al., 2013). The annual Horton Index is calculated as

$$HI = \frac{ET}{W}. \quad (2.8)$$

2.3.3 Analysis Hydrologic Metrics

Typical watershed hydrologic conditions are identified and compared using the mean to quantify central tendencies and the range and standard deviation to quantify variability. Correlations between similar metrics in different watersheds are quantified using the Pearson correlation coefficient. Interannual trends in hydrologic metrics are analyzed using linear regressions over the entire period of record as well as iteratively over all 30-year time spans to determine the consistency of the significance and extent of trends.

2.3.4 Prediction of Streamflow

The correlation between annual precipitation and annual streamflow is quantified using linear regression analysis. This analysis is performed using the combined data from every watershed to create one regression as well as by separating data by watershed to create seven unique regressions in order to compare partitioning between watersheds. This comparison is made to determine whether differences in precipitation completely

control streamflow response or if watershed landscape characteristics may influence partitioning.

After accounting for the correlation with precipitation, remaining streamflow variability is correlated to the hydrologic metrics in Table 2.2 through a multiple linear regression analysis that iteratively adds the metric with the most predictability until the R^2 of the correlation is improved by less than 0.03. Potential for collinearity in the hydrologic variables exists because the similarities between the variables may cause them to be correlated. However, while there may be statistical correlation between the variables, the factors all behave independently of each other on an annual basis and so they have the potential to account for unique variability in streamflow. Collinearity may cause multicollinearity in a multiple linear regression model. While multicollinearity does not affect the fit of the overall model, it can reduce the significance of individual variables and may affect the regression coefficients. Therefore, caution is used in interpreting the regression coefficients. Further analysis into the regression coefficients, not included in this thesis, should begin by analyzing the variance inflation factor for each of the multiple linear regressions.

2.3.5 Quantifying Winter Baseflow and Snowmelt Rate Variability

2.3.5.1 Background

Due to the significance of winter baseflow and snowmelt rate in the prediction of streamflow variability, I further explored the controls on these two variables in order to link them to watershed climate and landscape characteristics.

2.3.5.2 Winter Baseflow

I conduct a multiple linear regression analysis of winter baseflow for each watershed using hydrologic variables from the previous water years to predict the subsequent winter's baseflow. Hydrologic variables that are tested in this analysis included the antecedent September and October precipitation; previous annual, winter (November – April), and summer (May – October) precipitation; the percent of annual precipitation that occurred during the previous winter; previous average annual, winter (November – April), and summer (May – October) temperature; previous snowmelt rate, duration, start day, and end day; and the previous winter's baseflow. To account for lag effects that may extend past the previous year, all of these variables, except the antecedent September and October precipitation, are tested for 4 years previous to the winter baseflow. Variables that significantly correlate to winter baseflow ($p < 0.05$) and measurably reduce winter baseflow uncertainty ($R^2 > 0.05$) are included in the final multiple linear regression model.

2.3.5.3 Snowmelt Rate

Surface snowpack measurements are available at six locations throughout the watersheds, ranging in elevation from 2040 m to 2931 m, through the National Resource Conservation Service (NRCS) Snow Telemetry (SnoTel) observation sites (Figure 2.1) (NRCS National Water and Climate Center, 2017). The period of record for these sites varies because they were not all constructed during the same year: complete observations began in 1980 (Parley's Summit), 1988 (Brighton), 1989 (Lookout Peak), 1990 (Snowbird and MillD), and 2000 (Louis Meadow). In general, mean precipitation (870

mm – 1390 mm) and temperature (3.2°C– 6.2°C) at the SnoTel sites fall within or near the range of mean watershed values. Daily snow water equivalent (SWE) observations are used from each site's first year of record until 2014. The average of all six SnoTel sites provides a seventh data series. The daily surface snowmelt rate is calculated as the difference in SWE from one day to the next.

Annual surface snowmelt amount at each site is calculated as the peak SWE, in mm, for that year, using the assumption that all the snow that ablates after peak accumulation melts and that the majority of snowmelt from the snowpack occurs during this period. The number of days between the date of peak SWE and the date that SWE equals zero is the surface snowmelt duration. Dividing the surface snowmelt amount by the surface snowmelt duration provides the surface snowmelt rate, in mm/day. While similar to the snowmelt rate calculated for the entire watershed using daily streamflow observations, the surface snowmelt rate, calculated from SnoTel SWE observations, represents only the snowmelt processes as they occur at specific locations on the surface of the watersheds. A multiple linear regression analysis is used to compare the surface snowmelt rate with the watershed snowmelt rate. The remaining variability in this regression analysis is compared to the snowmelt amount and duration at both the SnoTel and watershed scale using a linear regression analysis.

2.3.6 Consideration of Vegetation Controls on Stored Water

Satellite imagery, through the moderate-resolution imaging spectroradiometer (MODIS) Normalized Difference Vegetation Index (NDVI) from the Global MOD13Q1 data, provides an opportunity to examine the vegetation response to climate conditions

and partitioning in the watersheds (MODIS, 2015). NDVI data are available in 16 day intervals at a spatial resolution of 250 meters during 2000 – 2014. Once downloaded, NDVI pixels are delineated by watershed. Additionally, a USGS Gap Land Cover raster from 2000 with 30 meter resolution is used to crop out non-vegetated land cover, including water bodies and rock outcroppings/talus slopes. NDVI pixel data are averaged over the entire watershed area for each 16-day time step. The peak NDVI value in each year for each watershed is used to estimate the maximum vegetation productivity during the growing season. NDVI values are analyzed similar to the analysis of the hydrologic metrics described above.

Annual vegetation productivity, represented by NDVI, is correlated to the annual Horton Index using linear regression analysis. Additionally, to compare the previous summer's vegetation productivity and the subsequent winter baseflow, I compare the peak NDVI value to the subsequent winter baseflow value using a linear regression analysis.

2.4 Results

2.4.1 Annual Climate and Landscape Features/Hydrology

2.4.1.1 Annual Precipitation

The mean annual precipitation ranges from 790 mm in PC to 1290 mm in LC (Table 2.3; Figure 2.2). Annual precipitation for each of the seven watersheds does not experience a significant ($p<0.05$) trend over time (Table 2.4).

Annual precipitation during the period of record covers substantial variability common throughout the Intermountain West, with precipitation ranging from 420 mm to

2135 mm. The standard deviation of annual precipitation varies, but is always between 20-21% of the mean. Interestingly, interannual variability within individual catchments overlaps from 740 mm to 1330 mm, meaning that every watershed had at least 1 year within this range of annual values. Interannual precipitation variability correlates between watersheds with Pearson R values between 0.93 – 1.00 (Table 2.5). The similarity of precipitation variability is expected since the watersheds are fairly close together and because of overlap in the PRISM data between watersheds.

2.4.1.2 Annual Temperature

The mean annual temperature ranges from 6.9°C in PC to 3.3°C in LC (Table 2.3; Figure 2.3). The watersheds experience differences in mean annual precipitation and temperature primarily are associated with elevation (Table 2.6). As shown in Table 2.3, the watershed (LC) with the highest annual precipitation had the lowest annual temperature. Conversely, the watershed (PC) with the lowest annual precipitation had the highest annual temperature.

Annual temperature during the period of record covers substantial variability common throughout the Intermountain West, with annual temperature ranging from 1.1°C to 9.9°C (Figure 2.3). The standard deviation of annual temperature is 0.8°C for all watersheds, except LC (0.9°C), indicating that watersheds exhibit similar interannual temperature variability (Table 2.3). All watersheds experience at least 1 year of overlap within the range of 4.9° C - 6.0°C. Similar to precipitation, the interannual temperature variability correlates between watersheds with Pearson R values between 0.93 – 1.00 (Table 2.5), which is expected since the watersheds receive similar regional climate

patterns and because of overlap in the PRISM data between watersheds.

A significant ($p<0.001$) warming trend (0.07° - 0.10°C / decade) exists in every watershed throughout the entire period of record, with the greatest rate of change between 1964 – 2014 (0.31° - 0.52°C) (Table 2.4).

2.4.1.3 Relative Humidity

Mean annual relative humidity is fairly similar between watersheds, ranging from 47% in PC to 51% in LC (Table 2.3). Figure 2.4 illustrates the interannual variability of relative humidity. No trend in relative humidity exists over the entire period of record ($p>0.05$). However, during the period of the greater rate of warming (1964 – 2014), relative humidity decreases significantly in every watershed with rates ranging from -0.8% to -1.8% / decade in PC and LC, respectively ($p<0.01$) (Table 2.4).

Annual relative humidity values during the period of record cover substantial variability common throughout the Intermountain West, ranging from 39% to 60% in MC and LC, respectively. All seven watersheds have a similar amount of variability around the mean during this period, with standard deviation between 3% - 4%. All watersheds experience at least 1 year of overlap within the annual relative humidity range of 40% and 53%. Interannual relative humidity variability correlates between watersheds with Pearson R values between 0.90 – 1.00 (Table 2.5).

2.4.1.4 Seasonal Results

Winter, spring, summer, and fall climate generally follows spatial and interannual temporal patterns that are similar to annual climate patterns (Table 2.7). Winter is the

wettest and coldest season: precipitation, on average, accounts for 33 – 37% of the annual total, relative humidity is typically 13 – 16% greater than the annual mean, and temperature is typically 9-10°C cooler than the annual mean (Figures 2.5-2.7). Spring is warmer, but nearly as wet as winter: precipitation, on average, accounts for 31 – 33% of the annual total, relative humidity is typically 1% less than the annual mean, and temperature is typically 2°C cooler than the annual mean. Summer is the driest and warmest season: precipitation, on average, accounts for 10-12% of the annual total, relative humidity is typically 11-13 percentage points less than the annual mean, and temperature is typically 10-11°C warmer than the annual mean. Summer precipitation has notably greater interannual variability ($0.51 > \text{coefficient of variation} > 0.45$) than annual or other seasonal precipitation. Fall is slightly warmer and drier than spring: precipitation, on average, accounts for 21-23% of the annual total, relative humidity is typically 1-2 percentage points less than the annual mean, and temperature is typically 1°C warmer than the annual mean.

An interannual warming trend over the entire period of record is significant for the spring, summer, and fall seasons ($p < 0.05$). Warming during spring and fall occurs at a similar rate to annual warming (0.07 – 0.10°C/decade), except in PC and BC during the spring where the trend is not significant at $p < 0.05$. Summer temperature increases at a slightly more rapid rate than annual warming (0.08 – 0.13°C/decade). In contrast, during the period from 1964 – 2014 when annual warming is most significant, the rate of increase in temperature is greatest during the spring (0.44 – 0.63°C/decade), similar to the annual rate during the summer (0.33 – 0.53°C/decade), and least during the winter (0.23 – 0.48°C/decade) and fall (0.21 – 0.41°C/decade).

2.4.1.5 Streamflow

Mean annual streamflow (normalized by watershed area) ranges from 147 mm in EC to 814 mm in LC (Table 2.3). Annual streamflow ranges from a minimum of 10 mm in EC to a maximum of 1570 mm in LC (Figure 2.8). The standard deviation of streamflow ranges from 27% in EC to 71% in LC of the mean respective streamflow, which is higher and more variable between watersheds than for precipitation or temperature (Table 2.3). Interannual streamflow is less correlated between watersheds (Pearson R: 0.83 – 0.98) than either precipitation or temperature (Table 2.5).

Interestingly, in spite of widespread warming over the last 50 years, there was no significant ($p<0.05$) trend in annual streamflow in any watershed (Table 2.4).

2.4.1.6 Winter Baseflow

Mean winter baseflow, defined as the average daily streamflow during December and January, ranges from 0.12 mm/day in EC to 0.53 mm/day in LC (Table 2.3). The total accumulated winter baseflow typically represents between 4% in LC – 10% in MC of annual streamflow. Streamflow is stable during the period classified as winter baseflow, with standard errors of the mean less than 3% of the mean streamflow during these months (Table 2.8).

Figure 2.9 presents the range and interannual variability in winter baseflow, ranging from 0.02 mm/day to 1.14 mm/day. The standard deviation of winter baseflow ranges from a low of 20% of the mean in EC and a high of 63% of the mean in CC. Correlation of interannual winter baseflow variability between watersheds is less than that of streamflow, with Pearson R ranging from 0.41 – 0.85 (Table 2.5). Winter

baseflow exhibits no significant trend over the entire period of record, except for a slight increase in LC (0.014 mm/day / decade, $p<0.05$) (Table 2.4). Interestingly, no trend in any watershed is significant during the period of greatest warming (1964-2014) (Table 2.4).

In four of the seven watersheds (RB, PC, BC, and LC), September and October precipitation preceding winter baseflow positively correlates ($0.11 < R^2 < 0.35$) to the winter baseflow, with slopes ranging from 2.3E-04 in RB to 7.7E-04 in BC (Table 2.9). In every watershed, the annual precipitation during the water year preceding winter baseflow correlates to the winter baseflow ($0.09 < R^2 < 0.38$). In five of the seven watersheds (CC, RB, PC, MC, and LC), the relationship is positive, with slopes ranging from 1.5E-05 in LC to 1.8E-04 in MC, while the relationship is negative in the remaining two, with a slope of -5.5E-05 in EC and -5.1E-05 in BC. Similarly, in all seven watersheds, snowmelt characteristics predict the subsequent winter baseflow. Snowmelt rate is important ($0.08 < R^2 < 0.17$) in six of the watersheds (CC, RB, EC, PC, MC, and BC), with a negative slope of -6.0E-3 in EC and positive slopes in the remaining five watersheds ranging from 6.6E-2 in PC to 2.2E-1 in MC. Snowmelt duration predicts subsequent winter baseflow ($0.06 < R^2 < 0.19$) in three watersheds (EC, BC, and LC) with a positive correlation ranging from 8.7E-4 in EC to 1.1E-3 in LC. Finally, in two watersheds, the antecedent winter baseflow predicts the following winter baseflow with a positive correlation of 0.39 in LC ($R^2 = 0.12$) and 0.50 in EC ($R^2 = 0.17$). Importantly, both antecedent annual and seasonal temperature did not add predictability to the winter baseflow.

2.4.1.7 Annual Snowmelt

The initiation and duration of snowmelt varies between watersheds, with snowmelt typically beginning earliest in RB (February 26) and latest in LC (April 5), and ending between July 30 (RB) and October 9 (MC) (Table 2.3; Figure 2.10). Snowmelt duration is shortest in LC (153 days) and longest in MC (201 days). On average, 67% - 83% of annual streamflow occurs during the snowmelt duration. The mean annual snowmelt rate ranges from 0.74 mm/day to 4.45 mm/day in EC and LC, respectively (Table 2.3; Figure 2.11).

The initiation of snowmelt is considerably less variable (standard deviation ranges from 14 days to 25 days) than the end of snowmelt (standard deviation ranges from 36 days to 70 days). The standard deviation of the snowmelt rate is between 23% in BC and 57% in EC of the respective watershed mean snowmelt rate.

Generally, warming temperature trends do not correspond to snowmelt trends. Snowmelt rate does not experience a significant trend over either the entire period of record or over the period of greatest warming (1964-2014) (Table 2.4). Five of the seven watersheds (CC, EC, PC, BC, and LC) experience a trend towards an earlier end of snowmelt during the entire period of record; however, only two (CC and PC) of these trends are also significant during the period of greatest warming. Conversely, one watershed, LC, experiences a trend toward a later end of snowmelt during the entire period of record. Only one watershed, PC, experiences a trend toward an earlier start of snowmelt during the entire period of record and only one watershed, LC, experiences a trend toward an earlier start of snowmelt during the period of greatest warming.

Surface snowmelt rate, derived from SnoTel observations, averages 16 mm/day

across the six SnoTel sites during the period of record, with the slowest snowmelt typically occurring at Louis Meadow (11 mm/day) and the fastest snowmelt typically occurring at Snowbird (25 mm/day) (Figure 2.12). Notably, these snowmelt rates are, in general, an order of magnitude greater than the watershed snowmelt rates calculated through daily streamflow analysis. The annual average snowmelt rate from all six SnoTel sites corresponds significantly ($p < 0.01$) with the watershed snowmelt rates from each watershed individually with slopes between 0.07 (CC) and 0.18 (LC) and R^2 values between 0.39 (LC) and 0.61 (MC) (Table 2.10). Remaining variability positively correlates to the observed snowmelt duration at the SnoTel sites (Table 2.11). The daily SnoTel maximum snowmelt rate annual pattern mirrors the annual pattern of incoming solar radiation with snowmelt rate decreasing from the fall to winter and subsequently increasing from the winter until the snowpack is completely ablated in the summer (Figure 2.13).

2.4.1.8 Annual Water Yield

Mean annual water yield, or the fraction of annual precipitation partitioned to streamflow (Q/P), ranges from 0.18 to 0.63 in EC and LC, respectively. Annual water yield ranges from 0.01 to 0.88, indicating that nearly any fraction of precipitation may be partitioned to streamflow during a single year (Figure 2.14). Interannual water yield variability between watersheds correlates less than that of precipitation, with Pearson R values ranging from 0.46 to 0.94 (Table 2.5). This is in contrast to strong coherence between catchments in precipitation (Pearson R values between 0.93 – 1.00).

Annual water yield exhibits no trend over time during the period of record within

five of the seven watersheds ($p>0.01$). However, the water yield decreased in BC throughout the entire period of study at a rate of -0.006/decade ($p = 0.011$) due primarily to a negative trend from 1906 to 1949 that averaged -0.04/decade. Conversely, the water yield increased in LC throughout the entire period of study at a rate of +0.007/decade ($p = 0.016$) due primarily to a positive trend from 1948 to 1988 that averaged +0.04/decade.

Watershed mean annual water yield significantly ($p < 0.01$) correlates to two of ten landscape characteristics: elevation and percent of area with rock outcrops (Table 2.12) with R^2 values of 0.73 and 0.82, respectively. Higher water yield correlates to watersheds with higher elevation and watersheds with a greater fraction of rock outcrop (i.e. watersheds with less vegetated area). The other landscape features, including aspect, steepness, and vegetation type, do not correlate to water yield. It should be noted, if LC is removed from this analysis, no significant correlation exists due to the limited elevation range and limited variability in rock outcrop.

2.4.1.9 Annual Evapotranspiration

Mean annual calculated evapotranspiration ranges from 470 mm in LC, with the highest mean elevation, to 680 mm in MC, with the third highest mean elevation, illustrating that evapotranspiration is not merely a function of watershed elevation (Table 2.13; Figure 2.15). Annual evapotranspiration ranges from a minimum of 157 mm in LC to a maximum of 1132 mm in MC (Figure 2.15). Within-watershed standard deviation of evapotranspiration is between 17% (RB) and 29% (LC) of the mean value (Table 2.13). Variability is not highly correlated between all watersheds, with Pearson R values ranging from 0.48 to 0.97 (Table 2.14). No trend over time exists in evapotranspiration,

except for a -11 mm/decade trend ($p = 0.017$) in LC during the entire period of record that is not significant ($p<0.05$) during the period of greatest warming (Table 2.15).

2.4.1.10 Annual Stormflow and Baseflow

Annual baseflow typically accounts for 80% - 90% of annual streamflow, while stormflow accounts for the other 10% - 20%. Annual stormflow and annual baseflow generally reflect streamflow patterns and trends. Mean annual baseflow ranges from 120 mm in EC – 650 mm in LC, while mean annual stormflow ranges from 20 mm in EC to 160 mm in LC (Table 2.13; Figures 2.16 and 2.17). The standard deviation of annual baseflow ranges from a low of 26% (LC) to a high of 71% (EC) of the mean and the standard deviation of annual stormflow range from a low of 31% (LC) to a high of 77% (EC) of the mean (Table 2.13). Variability between watersheds correlates similar to that of streamflow, with Pearson R values for annual baseflow between 0.81 and 0.98 and Pearson R values for annual stormflow between 0.88 and 0.96 (Table 2.14). No trend over time exists in annual baseflow or annual stormflow over the entire period of record or during the period of greatest warming (1964 – 2014), except in LC where a slightly significant ($p = 0.030$) decrease in annual stormflow exists from 1964 – 2014 (Table 2.15).

2.4.1.11 Annual Wetting

Annual wetting represents the annual amount of water added to a watershed available to vegetation, calculated as the difference between annual precipitation and annual stormflow. Mean annual wetting ranges from 760 mm in PC to 1120 mm in LC

(Table 2.13; Figure 2.18). Annual wetting ranges from a minimum of 416 mm in EC to a maximum of 1880 mm in LC (Figure 2.18). Wetting exhibits similar variability to precipitation in every watershed, with the standard deviation between 19% - 21% of the mean value in every watershed (Table 2.13). Pearson R values between 0.88 – 1.00 indicate that the correlation of interannual variability is also similar to precipitation (Table 2.14). No trend exists in wetting over the entire period of record or during the period of greatest warming (Table 2.15).

2.4.1.12 Annual Horton Index

The Horton Index represents the fraction of annual plant-available water partitioned to annual evapotranspiration, calculated as the annual evapotranspiration divided by annual wetting. Annual Horton Index ranges from 0.42 in LC to 0.85 in EC over the period of record (1902 – 2014) (Table 2.001; Figure 2.19). Standard deviation of mean watershed Horton Index values ranges from 0.06 in MC to 0.09 in EC (Table 2.13). Interannual variability correlates strongly between only a few of the watersheds, with Pearson R values ranging from 0.41 to 0.93 (Table 2.14). Horton Index increases in BC (+0.007 / decade; $p = 0.004$) over the entire period of record and in PC (+0.02 / decade; $p = 0.009$) and MC (+0.01 / decade; $p = 0.039$) over the period of greatest warming. Conversely, Horton Index decreases in LC (-0.007 / decade; $p = 0.014$) over the entire period of record (Table 2.15).

2.4.2 Prediction of Annual Streamflow

Annual streamflow significantly correlates to annual precipitation both on an aggregate watershed-basis and for individual watersheds, as illustrated in Figure 2.20. On an aggregate watershed-basis (shown as a dashed line in Figure 2.20), the expected streamflow initiation occurs at 526 mm of annual precipitation and increases by 0.84 mm for every mm increase in precipitation. Correlations between annual streamflow and annual precipitation within individual watersheds, also shown in Figure 2.20, illustrate differences in the streamflow and precipitation relationship between the seven watersheds. The expected amount of precipitation needed to induce streamflow ranges from 123 mm – 454 mm in BC and EC, respectively. Similarly, increase in streamflow per mm increase in precipitation ranges from 0.34 mm – 0.71 mm in MC and LC, respectively. These values are presented in Table 2.16 as the slope of the lines for each watershed in Figure 2.20.

Much of annual streamflow variability is correlated to precipitation in each watershed, with R^2 values for the correlation ranging from 0.44 to 0.73 in EC and LC, respectively, which represents the highest correlation of any metric in this analysis. However, considerable streamflow variability remains. Surprisingly, annual temperature does not add any predictability to streamflow after accounting for annual precipitation.

Multiple linear regression is used to determine other metrics that will contribute to improved streamflow prediction. Multiple linear regression analysis indicates that four metrics reduce annual streamflow uncertainty to less than 5% in every watershed (Figure 2.21 and Table 2.17). In all seven watersheds, three of these four metrics consist of annual precipitation, winter baseflow, and snowmelt rate. The snowmelt duration further

reduces uncertainty in all watersheds except RB, where it is replaced by the end date of snowmelt.

Similar to the varying degrees of predictability that precipitation adds to streamflow, R^2 values in Table 2.17 show that the variables added through the multiple linear regression analysis add different amounts of predictability to streamflow in the different watersheds: winter baseflow ranges from 0.06 in LC to 0.22 in MC, snowmelt rate ranges from 0.07 in LC to 0.25 in EC, snowmelt duration ranges from 0.04 in MC to 0.11 in LC, and snowmelt end date is 0.04 in RB. Also, correlation slopes for each of the variables in the multiple linear regressions, shown in Table 2.17, vary between watersheds. Therefore, the expected influence of a change in any one of these metrics on the resulting streamflow will also vary between watersheds. The 70 other hydro-climate metrics, from Table 2.2, that are analyzed in the multiple linear regression do not add significant predictability ($R^2 > 0.03$) to streamflow.

2.4.3 Vegetation Controls on Water Stored in the Subsurface

2.4.3.1 Annual Peak NDVI

Annual NDVI patterns in every watershed represent a substantial seasonal transition between winter and summer due to the land surface coverage of a winter snowpack (Figure 2.22). During the snow-free summer growing season, NDVI exhibits a smaller transition representative of spring vegetation green-up and summer/fall die-off. The timing of vegetation growth in the watersheds and the timing of streamflow's return to winter baseflow conditions from spring snowmelt suggest that vegetation may influence the amount of stored water in the subsurface carried over to the next water year.

Interannual NDVI variability is presented below through the annual peak NDVI, a simple and straightforward measure of vegetation greenness during the growing season.

Mean annual peak NDVI during the period of record (2000 – 2015) ranges from 0.61 in LC to 0.79 in RB (Figure 2.23). Each watershed experiences relatively minor interannual peak NDVI variability, with the standard deviations between 0.02 – 0.03 (Table 2.18). Variability between all the watersheds, however, does not correlate to a similar extent with Pearson R values ranging from 0.48 – 0.94 (Table 2.14). Throughout the 16 years of available NDVI data, three of the seven watersheds exhibit increasing peak NDVI over time ($p<0.05$): +0.02/decade in MC and +0.03/decade in BC and LC (Table 2.18). However, during this time period (2000 – 2014), there is no significant ($p<0.05$) trend in temperature data (Table 2.18).

Peak NDVI, a measure of vegetation greenness, positively correlates with subsequent winter baseflow in six of the seven watersheds (all except LC); however, the correlation is significant at $p<0.05$ in only two watersheds: CC ($p = 0.046$) and RB ($p = 0.030$) (Table 2.19).

2.4.3.2 NDVI and Horton Index Correlation

The correlation between peak NDVI and the Horton Index, illustrated in Figure 2.24, generally shows that in general, vegetation in wetter watersheds (those with lower Horton Index values) shows less of a response to drying than in drier watersheds, with slopes ranging from 0.006 in LC to -0.24 in PC (Table 2.20). However, this correlation is not significant at $p<0.01$ in any of the watersheds, with p values ranging from 0.03 in PC to 0.97 in MC.

2.5 Discussion

2.5.1 Factors Affecting Streamflow in Study Area Watersheds

The spatial correlation between annual watershed precipitation, temperature, and relative humidity of the watersheds to the east of Salt Lake City, Utah evaluated in this study suggests that the watersheds experience similar climate regimes. In the absence of clear understanding of how catchments may differentially impact partitioning in response to future climate change, water resource predictions are made that implicitly assume that watersheds within a certain region all behave along a single climate-controlled continuum (Barnett et al., 2005; N. S. Christensen et al., 2004; Milly et al., 2005). The difference in mean annual values between the sites makes them an ideal setting to test whether watersheds with historically warmer temperatures can be considered adequate analogues for the hydrologic behavior of watersheds that may experience warming in the future. Overlap in the range of annual climate conditions provides an opportunity to test whether the watersheds have similar hydrologic responses to similar climate forcing.

Multiple lines of evidence suggest that these watersheds do not all partition precipitation similarly. First, tremendous differences in water yield values and streamflow variability, even though watersheds have similar climate variability and some have similar climate conditions, indicates that the fraction of precipitation partitioned to streamflow varies between watersheds. Similar regional climate forcing between all the watersheds supports the hypothesis that watershed characteristics cause differential partitioning of precipitation (Croft, 1944b; Geroy et al., 2011; Zapata-Rios et al., 2015). Landscape characteristics such as elevation and vegetated area may explain some of the differences in water yield due to their influence on evapotranspiration and the amount

and type of precipitation (Table 2.12) (Hunsaker et al., 2012). Importantly, though, no individual landscape characteristic fully explains the variability between watersheds.

Tremendous differences in streamflow standard deviation relative to the mean, even though all watersheds have similar precipitation standard deviation relative to the mean, indicates that streamflow response to changes in precipitation varies between watersheds. Furthermore the significant variation in incremental water yield (the mm increase in streamflow for every mm increase in precipitation), ranging from 0.34 to 0.71, indicates that other factors influence streamflow.

Finally, no simple climate metric adds considerable predictability to streamflow in addition to annual precipitation. Instead, one landscape-controlled variable (winter baseflow), and three variables controlled by a combination of climate and landscape (snowmelt rate, snowmelt duration, and last day of snowmelt) further reduce streamflow uncertainty to less than 5% in every watershed. In addition to significantly correlating ($p < 0.05$) statistically to streamflow, each of these variables, as discussed below, has a physical basis for adding unique predictability to streamflow. This implies that a robust prediction of the hydrologic response that may occur as a result of a shift in long-term precipitation cannot be made simply by assuming a response similar to other watersheds with climate conditions analogous to those that may be forcing the watershed in the future. Rather, projections of hydrologic response to future climate change must stem from research that quantifies the demands on subsurface water available to baseflow and relates snowmelt processes to hydrologic partitioning (Barnhart et al., 2016; Croft, 1946; Deshmukh & Singh, 2016).

2.5.2 Temperature and Hydrologic Partitioning

Surprisingly, temperature does not add predictability to annual streamflow after accounting for precipitation. Similarly, historic warming trends and the related decreases in relative humidity in all watersheds do not result in subsequent trends in streamflow, evapotranspiration, or hydrologic partitioning (Table 2.4). This indicates that historic partitioning displays no direct, identifiable response to temperature trends or variability during the time frames considered, contrary to the modeled future impact that temperature will have on streamflow in these specific watersheds and similar watersheds throughout the Western United States (Bardsley et al., 2013; Barnett et al., 2005). Due to the importance of snowmelt metrics and winter baseflow on streamflow in every watershed, the effects of a warming climate on annual streamflow should be addressed through energy budget changes to the snowpack, especially as it melts (Foster et al., 2016), and through multiyear water balance changes affecting the level of available stored water (Brooks et al., 2015).

2.5.3 Baseflow and Streamflow Generation

I identify a simple, transferable metric, winter baseflow, which represents the relative amount of available stored water and correlates to streamflow in all the study watersheds (Wittenberg & Sivapalan, 1999). Typically, streamflow is expected to be a combination of concurrent climate conditions and a memory of previous climate conditions through the release of water stored in the watershed (Hornberger et al., 2014). However, the intra-annual stability of winter baseflow confirms the expected dissociation between streamflow and concurrent climate conditions during the months of December

and January (Table 2.8). Throughout various climates and geophysical regions, research strongly suggests that the majority of stream water, even during storm events, has interacted with the subsurface for a substantial period of time, rather than primarily running over the surface to a stream channel (Godsey et al., 2009; Kirchner, 2003). Hydrologic modelers often account for available subsurface water through intensive measurements focused entirely on soil moisture (Croft, 1946; McNamara et al., 2005; Yaseef et al., 2010). However, studies of subsurface storage generally lack precise and transferable definitions, methods, and metrics that can be readily applied to capture processes at a watershed scale (McNamara, 2011). Differences in the patterns of winter baseflow between watersheds with similar climate patterns reflect differences in vegetation and subsurface characteristics that control the amount of water that can be stored in a watershed's subsurface and the residence time of the stored water (Wittenberg & Sivapalan, 1999; Zhang et al., 2016). Therefore, a watershed's correlation to winter baseflow indicates the system's ability to buffer annual climate variability and the importance of antecedent climate effects on future hydrologic response (Potter & Zhang, 2007). For example, in LC, where winter baseflow explains only 6% of streamflow variability, the effects of changes to climate conditions that influence the partitioning of stored water will impact streamflow much less than the effects of similar changes in MC, where winter baseflow explains 22% of streamflow variability (Table 2.17).

Due to the significance of winter baseflow in the prediction of streamflow variability (Table 2.17), I further explored the controls on winter baseflow in order to link it to watershed climate and landscape characteristics. Winter baseflow, indicative of catchment storage, primarily reflects antecedent precipitation and the fate of snowmelt

from the previous spring (Table 2.9). The influence of these two factors on winter baseflow may extend more than 1 year past when they occur due to the importance of 1 year's winter baseflow predicting the next year's winter baseflow in two of the watersheds. Patterns of the influence of precipitation on winter baseflow do not appear to relate to watershed characteristics. However, the importance of September and October precipitation in two watersheds suggests that the seasonal decrease in atmospheric demands may allow for preferential partitioning of fall precipitation to streamflow (Croft, 1946). The importance of the partitioning of snowmelt on winter baseflow further highlights the critical role of factors that influence catchment-scale melt processes.

Due to the large fraction of precipitation partitioned to evapotranspiration in many watersheds, vegetation productivity has been suggested to be a controlling factor of the partitioning in subsurface storage (Brooks et al., 2015; McDowell et al., 2008; Peel, 2009). Using the Horton Index, Brooks et al. (2011) characterized catchments with a Horton Index less than 0.66 as energy-limited and greater than 0.66 as water-limited, thereby identifying watersheds where vegetation productivity is more likely to control the partitioning of subsurface water. However, the substantial uncertainty in the relationship between NDVI and HI throughout these seven watersheds (Table 2.20) suggests that vegetation productivity does not significantly correlate to concurrent water availability alone, even in RB, EC, PC, and MC where the Horton Index suggests vegetation is water-limited. One alternate hypothesis is that partitioning may be dependent on the size, relative fullness, and residence time of the catchment groundwater aquifer. Therefore, the effects of annual climate variability on concurrent year vegetation timing and productivity may be ineffective at completely capturing subsurface storage variability and

the resulting streamflow response. Vegetation greenness positively correlates with winter baseflow in six of the seven watersheds, suggesting that similar factors may control the supply of water to both atmospheric demands and baseflow generation while, at the same time, the atmospheric demand may not substantially deplete the amount of water available to baseflow generation.

2.5.4 Snowmelt Rate and Streamflow Generation

In all watersheds, snowmelt rate is an important control on streamflow variability. Snowmelt timing, represented by snowmelt duration in six watersheds and the snowmelt end date in the seventh, is also important in every watershed. Once the snowpack absorbs enough energy in the spring to reach 0°C, most of the snow ablates through melting, rather than sublimating or evaporating (Croft, 1944a; Hood et al., 1999). Previous studies have shown that the nearly all of the snowmelt infiltrates into subsurface (Croft, 1944b). Once in the subsurface, the snowmelt generally seeps downward through the shallow subsurface (vadose zone) until reaching saturation (infiltration-excess), which allows the water to flow laterally through the subsurface (Barnhart et al., 2016; McNamara et al., 2005). Therefore, a snowpack with a fast melt rate can bring the soil to its infiltration-excess capacity more quickly than a slowly-melting snowpack, resulting in more efficient lateral vs. vertical movement of the snowmelt (Barnhart et al., 2016). The activation of shallow flowpaths through a faster snowmelt leads to a relative increase in streamflow during the concurrent year (Tague et al., 2008). This suggests that snowmelt-driven subsurface partitioning is a significant streamflow-generation process in watersheds that spans a wide range of seasonal snowpack conditions and subsurface landscape

characteristics (Molotch et al., 2009; Seyfried et al., 2009). The groundwater depth, aspect-controlled soil moisture content, and subsurface hydraulic conductivity can differentially affect the sensitivity of these snowmelt-induced flowpaths (Hinckley et al., 2014; Liu et al., 2013; Tague et al., 2008).

Due to the significance of snowmelt rate in the prediction of streamflow variability (Table 2.17), I further explored the controls on snowmelt rate in order to link it to watershed climate and landscape characteristics. Snowmelt occurs at a much faster rate at the SnoTel sites compared to the watershed snowmelt rate (derived from streamflow observations). Difference between SnoTel and watershed may be due to greater snowfall totals at the SnoTel sites compared to mean watershed snowfall as SnoTel sites generally over-represent high accumulation areas and the SnoTel sites are located well above mean watershed elevations (Molotch & Bales, 2006). However, such factors do not account for differences on the scale of an order of magnitude, with the remaining difference likely accounted for by the storage and transmittance of the snowmelt through the subsurface (McNamara et al., 2005). A longer SnoTel snowmelt duration results in a faster watershed snowmelt rate than expected when compared to the SnoTel snowmelt rate (Table 2.11). This relationship suggests that a longer melt increases subsurface saturation, resulting in increased groundwater connectivity and snowmelt-induced streamflow, thus increasing the watershed snowmelt rate.

Energy from solar radiation is the primary control on the intra-annual snowmelt rate, with the maximum melt rate increasing throughout the spring and summer due to the increase in incoming solar radiation (Figure 2.13) (DeWalle & Rango, 2008). Therefore, snowpacks that exist later into the spring or summer will melt faster than those that ablate

earlier in the year. Consequently, interannual winter precipitation amount variability will impact the snowmelt rate, as larger snowpack will typically persist later in the year than smaller snowpack. This may help to explain why precipitation correlation with winter baseflow varies from positive to negative between watersheds (Table 2.9) because, while more precipitation increases the supply of water available to be partitioned to baseflow, more precipitation also causes a later, and hence faster, snowmelt, which preferentially partitions water to streamflow rather than to stored water available to baseflow generation.

Snowmelt is physically driven by energy input into a ripe snowpack. Variable climate conditions affect the energy balance during the snowmelt period. For example, more winter snowfall can lead to a snowpack that peaks and lasts later into the spring and summer when daily solar radiation is greater (Trujillo & Molotch, 2014), warmer temperatures can shift melt timing to earlier in the spring when there is less solar radiation and lower the melt rate (Clow, 2009; Harpold et al., 2012), and increased humidity can add energy to the snowpack through longwave radiation and latent heat transfer from increased condensation onto the snowpack. Future climate change has the potential to affect snowmelt rate and timing. However, the lack of a trend in the timing or rate of melt to correspond with an increase in temperature suggests that there may be feedbacks between the effect of temperature and humidity on the melting snowpack that are not yet fully understood or that the increase in temperature is not yet significant enough to cause a shift in snowmelt to exceed natural variability. Watershed characteristics that affect the surface energy balance, such as elevation, slope aspect, hillshading, and vegetation shading, have been linked to snowmelt rate (Lyon et al.,

2008; Molotch et al., 2009; Rinehart et al., 2008). As a result, the sensitivity of snowmelt rate and timing to future climate change will vary.

2.6 References

Alduchov, O. A., & Eskridge, R. E. (1996). Improved magnus form approximation of saturation vapor pressure. *Journal of Applied Meteorology*, *35*(4), 601–609. https://doi.org/10.1175/1520-0450(1996)035<0601:IMFAOS>2.0.CO;2

Anderson, L. R., Keaton, J. R., Saarineri, T. F., & Wells, W. G. (1984). *The Utah landslides, debris flows, and floods of May and June 1983* (No. CETS-CND-025) (p. 108). Washington, D.C.: National Academy Press.

Armstrong, R. L., & Armstrong, B. R. (1987). Snow and avalanche climates of the western United States: A comparison of maritime, intermountain and continental conditions. *IAHS Publication*, *162 (1987)*, 281–294.

Arnell, N. W. (1999). Climate change and global water resources. *Global Environmental Change*, *9*, *Supplement 1*, S31–S49. https://doi.org/10.1016/S0959-3780(99)00017-5

Arnell, N. W. (2004). Climate change and global water resources: SRES emissions and socio-economic scenarios. *Global Environmental Change*, *14*(1), 31–52. https://doi.org/10.1016/j.gloenvcha.2003.10.006

Atwood, W. W. (1909). *Glaciation of the Uinta and Wasatch Mountains* (USGS Numbered Series No. 61) (p. 96). Washington: US Geological Survey. Retrieved from https://pubs.usgs.gov/pp/0061/report.pdf

Bales, R. C., Molotch, N. P., Painter, T. H., Dettinger, M. D., Rice, R., & Dozier, J. (2006). Mountain hydrology of the western United States. *Water Resources Research*, *42*(8), W08432. https://doi.org/10.1029/2005WR004387

Bardsley, T., Wood, A., Hobbins, M., Kirkham, T., Briefer, L., Niermeyer, J., & Burian, S. (2013). Planning for an uncertain future: Climate change sensitivity assessment toward adaptation planning for public water supply. *Earth Interactions*, *17*(23), 1–26. https://doi.org/10.1175/2012EI000501.1

Barnett, T. P., Adam, J. C., & Lettenmaier, D. P. (2005). Potential impacts of a warming climate on water availability in snow-dominated regions. *Nature*, *438*(7066), 303–309. https://doi.org/10.1038/nature04141

Barnett, T. P., & Pierce, D. W. (2008). When will Lake Mead go dry? *Water Resources Research*, *44*(3), W03201. https://doi.org/10.1029/2007WR006704

Barnett, T. P., Pierce, D. W., Hidalgo, H. G., Bonfils, C., Santer, B. D., Das, T., … Dettinger, M. D. (2008). Human-induced changes in the hydrology of the Western United States. *Science*, *319*(5866), 1080–1083. https://doi.org/10.1126/science.1152538

Barnhart, T. B., Molotch, N. P., Livneh, B., Harpold, A. A., Knowles, J. F., & Schneider, D. (2016). Snowmelt rate dictates streamflow. *Geophysical Research Letters*, *43*(15), 2016GL069690. https://doi.org/10.1002/2016GL069690

Bates, B., Kundzewicz, Z. W., Wu, S., & Palutikof, J. (2008). *Climate change and water* (Technical Paper of the Intergovernmental Panel on Climate Change) (p. 210). Geneva: IPCC Secretariat.

Bazemore, D. E., Eshleman, K. N., & Hollenbeck, K. J. (1994). The role of soil water in stormflow generation in a forested headwater catchment: Synthesis of natural tracer and hydrometric evidence. *Journal of Hydrology*, *162*(1), 47–75. https://doi.org/10.1016/0022-1694(94)90004-3

Beven, K. (2006). Searching for the Holy Grail of scientific hydrology: Qt=(S, R, Δt)A as closure. *Hydrologic Earth System Science*, *10*(5), 609–618. https://doi.org/10.5194/hess-10-609-2006

Biederman, J. A., Somor, A. J., Harpold, A. A., Gutmann, E. D., Breshears, D. D., Troch, P. A., … Brooks, P. D. (2015). Recent tree die-off has little effect on streamflow in contrast to expected increases from historical studies. *Water Resources Research*, *51*(12), 9775–9789. https://doi.org/10.1002/2015WR017401

Biek, B., Willis, G., & Ehler, B. (2010). Utah's glacial geology. *Survey Notes: Utah Geological Survey*, *42*(3), 1–4.

Bosch, J. M., & Hewlett, J. D. (1982). A review of catchment experiments to determine the effect of vegetation changes on water yield and evapotranspiration. *Journal of Hydrology*, *55*(1), 3–23. https://doi.org/10.1016/0022-1694(82)90117-2

Bowles, D., Hughes, T., James, W., Jensen, D., & Haws, F. (1980). Vulnerability of water supply systems to droughts, (Paper 587). Retrieved from http://digitalcommons.usu.edu/water_rep/587

Brooks, P. D., Chorover, J., Fan, Y., Godsey, S. E., Maxwell, R. M., McNamara, J. P., & Tague, C. (2015). Hydrological partitioning in the critical zone: Recent advances and opportunities for developing transferable understanding of water cycle dynamics. *Water Resources Research*, *51*(9), 6973–6987. https://doi.org/10.1002/2015WR017039

Brooks, P. D., Troch, P. A., Durcik, M., Gallo, E., & Schlegel, M. (2011). Quantifying regional scale ecosystem response to changes in precipitation: Not all rain is created equal. *Water Resources Research*, *47*(10), W00J08. https://doi.org/10.1029/2010WR009762

Burnham, M., Ma, Z., Endter-Wada, J., & Bardsley, T. (2016). Water management decision making in the face of multiple forms of uncertainty and risk. *Journal of the American Water Resources Association*, *52*(6), 1366–1384. https://doi.org/10.1111/1752-1688.12459

Canadell, J., Jackson, R. B., Ehleringer, J. B., Mooney, H. A., Sala, O. E., & Schulze, E.-D. (1996). Maximum rooting depth of vegetation types at the global scale. *Oecologia*, *108*(4), 583–595. https://doi.org/10.1007/BF00329030

Cayan, D. R., Dettinger, M. D., Kammerdiener, S. A., Caprio, J. M., & Peterson, D. H. (2001). Changes in the onset of spring in the Western United States. *Bulletin of the American Meteorological Society*, *82*(3), 399–415. https://doi.org/10.1175/1520-0477(2001)082<0399:CITOOS>2.3.CO;2

Cayan, D. R., Maurer, E. P., Dettinger, M. D., Tyree, M., & Hayhoe, K. (2008). Climate change scenarios for the California region. *Climatic Change*, *87*(1), 21–42. https://doi.org/10.1007/s10584-007-9377-6

Chase, K. J., Haj, A. E., Regan, R. S., & Viger, R. J. (2016). Potential effects of climate change on streamflow for seven watersheds in eastern and central Montana. *Journal of Hydrology: Regional Studies*, *7*, 69–81. https://doi.org/10.1016/j.ejrh.2016.06.001

Christensen, L., Tague, C. L., & Baron, J. S. (2008). Spatial patterns of simulated transpiration response to climate variability in a snow dominated mountain ecosystem. *Hydrological Processes*, *22*(18), 3576–3588. https://doi.org/10.1002/hyp.6961

Christensen, N. S., Wood, A. W., Voisin, N., Lettenmaier, D. P., & Palmer, R. N. (2004). The effects of climate change on the hydrology and water resources of the Colorado River Basin. *Climatic Change*, *62*(1–3), 337–363. https://doi.org/10.1023/B:CLIM.0000013684.13621.1f

Clow, D. W. (2009). Changes in the timing of snowmelt and streamflow in Colorado: A response to recent warming. *Journal of Climate*, *23*(9), 2293–2306. https://doi.org/10.1175/2009JCLI2951.1

Croft, A. R. (1944a). Snow melting and evaporation. *Science*, *100*(2591), 169–170.

Croft, A. R. (1944b). Some recharge- and discharge-phenomena of north- and south-facing watershed-lands in the Wasatch Mountains. *Eos, Transactions American Geophysical Union*, *25*(6), 881–889. https://doi.org/10.1029/TR025i006p00881

Croft, A. R. (1946). Some factors that influence the accuracy of water-supply forecasting in the intermountain region. *Eos, Transactions American Geophysical Union*, *27*(3), 375–388. https://doi.org/10.1029/TR027i003p00375

Croft, A. R., & Monninger, L. V. (1953). Evapotranspiration and other water losses on some aspen forest types in relation to water available for stream flow. *Eos, Transactions American Geophysical Union*, *34*(4), 563–574. https://doi.org/10.1029/TR034i004p00563

Daly, C., Halbleib, M., Smith, J. I., Gibson, W. P., Doggett, M. K., Taylor, G. H., … Pasteris, P. P. (2008). Physiographically sensitive mapping of climatological temperature and precipitation across the conterminous United States. *International Journal of Climatology*, *28*(15), 2031–2064. https://doi.org/10.1002/joc.1688

Deshmukh, A., & Singh, R. (2016). Physio-climatic controls on vulnerability of watersheds to climate and land use change across the U. S. *Water Resources Research*, *52*(11), 8775–8793. https://doi.org/10.1002/2016WR019189

DeWalle, D. R., & Rango, A. (2008). *Principles of snow hydrology*. Cambridge, UK: Cambridge University Press.

Dingman, S. L. (1981). Elevation: A major influence on the hydrology of New Hampshire and Vermont, USA. *Hydrological Sciences Bulletin*, *26*(4), 399–413. https://doi.org/10.1080/02626668109490904

Ehleringer, J. R. (1988). Changes in leaf characteristics of species along elevational gradients in the Wasatch Front, Utah. *American Journal of Botany*, *75*(5), 680–689. https://doi.org/10.2307/2444201

Ehleringer, J. R., Arnow, L. A., Arnow, T., McNulty, I. B., & Negus, N. C. (1992). Red Butte Canyon Research Natural Area: History, flora, geology, climate, and ecology. *The Great Basein Naturalist*, *52*(2), 95–121.

Ehlers, T. A., Willett, S. D., Armstrong, P. A., & Chapman, D. S. (2003). Exhumation of the central Wasatch Mountains, Utah: 2. Thermokinematic model of exhumation, erosion, and thermochronometer interpretation. *Journal of Geophysical Research: Solid Earth*, *108*(B3), 2173. https://doi.org/10.1029/2001JB001723

Foster, L. M., Bearup, L. A., Molotch, N. P., Brooks, P. D., & Maxwell, R. M. (2016). Energy budget increases reduce mean streamflow more than snow–rain transitions: Using integrated modeling to isolate climate change impacts on Rocky Mountain hydrology. *Environmental Research Letters*, *11*(4), 044015. https://doi.org/10.1088/1748-9326/11/4/044015

Fowler, H. J., Blenkinsop, S., & Tebaldi, C. (2007). Linking climate change modelling to impacts studies: Recent advances in downscaling techniques for hydrological modelling. *International Journal of Climatology*, *27*(12), 1547–1578. https://doi.org/10.1002/joc.1556

Frisbee, M. D., Phillips, F. M., Weissmann, G. S., Brooks, P. D., Wilson, J. L., Campbell, A. R., & Liu, F. (2012). Unraveling the mysteries of the large watershed black

box: Implications for the streamflow response to climate and landscape perturbations. *Geophysical Research Letters*, *39*(1), L01404. https://doi.org/10.1029/2011GL050416

Garfin, G., Jardine, A., Merideth, R., Black, M., & LeRoy, S. (2013). *Assessment of climate change in the southwest United States: A report prepared for the National Climate Assessment*. Washington, DC: Island Press.

Geroy, I. J., Gribb, M. M., Marshall, H. P., Chandler, D. G., Benner, S. G., & McNamara, J. P. (2011). Aspect influences on soil water retention and storage. *Hydrological Processes*, *25*(25), 3836–3842. https://doi.org/10.1002/hyp.8281

Gleick, P. H. (1989). Climate change, hydrology, and water resources. *Reviews of Geophysics*, *27*(3), 329–344. https://doi.org/10.1029/RG027i003p00329

Gleick, P. H. (2003). Water use. *Annual Review of Environment and Resources*, *28*(1), 275–314. https://doi.org/10.1146/annurev.energy.28.040202.122849

Godsey, S. E., Kirchner, J. W., & Clow, D. W. (2009). Concentration–discharge relationships reflect chemostatic characteristics of US catchments. *Hydrological Processes*, *23*(13), 1844–1864. https://doi.org/10.1002/hyp.7315

Gosling, S. N., & Arnell, N. W. (2016). A global assessment of the impact of climate change on water scarcity. *Climatic Change*, *134*(3), 371–385. https://doi.org/10.1007/s10584-013-0853-x

Granger, A. E. (1953). *Stratigraphy of the Wasatch Range near Salt Lake City, Utah* (USGS Numbered Series No. 296). U.S. Geological Survey. Retrieved from http://pubs.er.usgs.gov/publication/cir296

Hamlet, A. F., Mote, P. W., Clark, M. P., & Lettenmaier, D. P. (2005). Effects of temperature and precipitation variability on snowpack trends in the western United States. *Journal of Climate*, *18*(21), 4545–4561. https://doi.org/10.1175/JCLI3538.1

Harpold, A., Brooks, P., Rajagopal, S., Heidbuchel, I., Jardine, A., & Stielstra, C. (2012). Changes in snowpack accumulation and ablation in the intermountain west. *Water Resources Research*, *48*(11), W11501. https://doi.org/10.1029/2012WR011949

Hassan, F. A. (2010). *Water history for our times*. Paris: United Nations Educational, Scientific and Cultural Organization.

Hely, A. G., Mower, R. W., Harr, C. A., & Arnow, T. (1971). *Water resources of Salt Lake County, Utah* (Other Government Series No. 31) (p. 240). Salt Lake City, UT: Utah Department of Natural Resources, Division of Water Rights.

Hinckley, E. L. S., Ebel, B. A., Barnes, R. T., Anderson, R. S., Williams, M. W., & Anderson, S. P. (2014). Aspect control of water movement on hillslopes near the

rain–snow transition of the Colorado Front Range. *Hydrological Processes*, *28*(1), 74–85. https://doi.org/10.1002/hyp.9549

Hirabayashi, Y., Mahendran, R., Koirala, S., Konoshima, L., Yamazaki, D., Watanabe, S., … Kanae, S. (2013). Global flood risk under climate change. *Nature Climate Change*, *3*. https://doi.org/10.1038/nclimate1911

Hollis, G. E. (1975). The effect of urbanization on floods of different recurrence interval. *Water Resources Research*, *11*(3), 431–435. https://doi.org/10.1029/WR011i003p00431

Hood, E., Williams, M., & Cline, D. (1999). Sublimation from a seasonal snowpack at a continental, mid-latitude alpine site. *Hydrological Processes*, *13*(12–13), 1781–1797. https://doi.org/10.1002/(SICI)1099-1085(199909)13:12/13<1781::AID-HYP860>3.0.CO;2-C

Hornberger, G. M., Wiberg, P. L., Raffensperger, J. P., & D'Odorico, P. (2014). *Elements of physical hydrology* (2nd ed.). Baltimore, MD: Johns Hopkins University Press.

Horton, R. E. (1933). The rôle of infiltration in the hydrologic cycle. *Eos, Transactions American Geophysical Union*, *14*(1), 446–460. https://doi.org/10.1029/TR014i001p00446

Hughes, T., Bigler, C., Olds, J., Griffin, R., Richardson, A., James, L., … Harvey, J. (1978). Utah's 1977 drought. *Reports*, (Paper 395). Retrieved from http://digitalcommons.usu.edu/water_rep/395

Hunsaker, C. T., Whitaker, T. W., & Bales, R. C. (2012). Snowmelt runoff and water yield along elevation and temperature gradients in California's southern Sierra Nevada. *Journal of the American Water Resources Association*, *48*(4), 667–678. https://doi.org/10.1111/j.1752-1688.2012.00641.x

Juuti, P. S., Katko, T. S., & Vuorinen, H. S. (2007). *Environemtal history of water: Global views on community water supply and sanitation*. London: IWA Publishing.

Kirchner, J. W. (2003). A double paradox in catchment hydrology and geochemistry. *Hydrological Processes*, *17*(4), 871–874. https://doi.org/10.1002/hyp.5108

Kirchner, J. W. (2006). Getting the right answers for the right reasons: Linking measurements, analyses, and models to advance the science of hydrology. *Water Resources Research*, *42*(3), W03S04. https://doi.org/10.1029/2005WR004362

Knowles, N., Dettinger, M. D., & Cayan, D. R. (2006). Trends in snowfall versus rainfall in the western United States. *Journal of Climate*, *19*(18), 4545–4559. https://doi.org/10.1175/JCLI3850.1

Lawrence, M. G. (2005). The relationship between relative humidity and the dewpoint temperature in moist air: A simple conversion and applications. *Bulletin of the American Meteorological Society*, *86*(2), 225–233. https://doi.org/10.1175/BAMS-86-2-225

Liu, F., Hunsaker, C., & Bales, R. C. (2013). Controls of streamflow generation in small catchments across the snow–rain transition in the Southern Sierra Nevada, California. *Hydrological Processes*, *27*(14), 1959–1972. https://doi.org/10.1002/hyp.9304

Lyne, V., & Hollick, M. (1979). Stochastic time-variable rainfall-runoff modelling. *Hydrology and Water Resources Symposium, Institution of Engineers Australia National Conference*, 89–93.

Lyon, S. W., Troch, P. A., Broxton, P. D., Molotch, N. P., & Brooks, P. D. (2008). Monitoring the timing of snowmelt and the initiation of streamflow using a distributed network of temperature/light sensors. *Ecohydrology*, *1*(3), 215–224. https://doi.org/10.1002/eco.18

Manning, A. H., & Solomon, D. K. (2005). An integrated environmental tracer approach to characterizing groundwater circulation in a mountain block. *Water Resources Research*, *41*(12), W12412. https://doi.org/10.1029/2005WR004178

Maraun, D., Wetterhall, F., Ireson, A. M., Chandler, R. E., Kendon, E. J., Widmann, M., … Thiele-Eich, I. (2010). Precipitation downscaling under climate change: Recent developments to bridge the gap between dynamical models and the end user. *Reviews of Geophysics*, *48*(3), RG3003. https://doi.org/10.1029/2009RG000314

Maurer, E. P., & Duffy, P. B. (2005). Uncertainty in projections of streamflow changes due to climate change in California. *Geophysical Research Letters*, *32*(3), L03704. https://doi.org/10.1029/2004GL021462

Mayer, T. D., & Naman, S. W. (2011). Streamflow response to climate as influenced by geology and elevation. *Journal of the American Water Resources Association*, *47*(4), 724–738. https://doi.org/10.1111/j.1752-1688.2011.00537.x

McDowell, N. G., White, S., & Pockman, W. T. (2008). Transpiration and stomatal conductance across a steep climate gradient in the southern Rocky Mountains. *Ecohydrology*, *1*(3), 193–204. https://doi.org/10.1002/eco.20

McNamara, J. P., Chandler, D., Seyfried, M., & Achet, S. (2005). Soil moisture states, lateral flow, and streamflow generation in a semi-arid, snowmelt-driven catchment. *Hydrological Processes*, *19*(20), 4023–4038. https://doi.org/10.1002/hyp.5869

McNamara, J. P., Tetzlaff, D., Bishop, K., Soulsby, C., Seyfried, M., Peters, N. E., … Hooper, R. (2011). Storage as a metric of catchment comparison. *Hydrological Processes*, *25*(21), 3364–3371. https://doi.org/10.1002/hyp.8113

Meehl, G. A., Covey, C., Taylor, K. E., Delworth, T., Stouffer, R. J., Latif, M., … Mitchell, J. F. B. (2007). THE WCRP CMIP3 multimodel dataset: A new era in climate change research. *Bulletin of the American Meteorological Society, 88*(9), 1383–1394. https://doi.org/10.1175/BAMS-88-9-1383

Milly, P. C. D., Betancourt, J., Falkenmark, M., Hirsch, R. M., Kundzewicz, Z. W., Lettenmaier, D. P., & Stouffer, R. J. (2008). Stationarity is dead: Whither water management? *Science, 319*(5863), 573–574. https://doi.org/10.1126/science.1151915

Milly, P. C. D., Dunne, K. A., & Vecchia, A. V. (2005). Global pattern of trends in streamflow and water availability in a changing climate. *Nature, 438*(7066), 347–350. https://doi.org/10.1038/nature04312

MODIS. (2015). *Terra MODIS ver. 5, Vegetation indices 16-day L3 global 250m*. Sioux Falls, South Dakota: NASA EOSDIS Land Processes DAAC, USGS Earth Resources Observation and Science (EROS) Center. Retrieved from https://lpdaac.usgs.gov/dataset_discovery/modis/modis_products_table/mod13q1

Molotch, N. P., & Bales, R. C. (2006). SNOTEL representativeness in the Rio Grande headwaters on the basis of physiographics and remotely sensed snow cover persistence. *Hydrological Processes*, *20*(4), 723–739. https://doi.org/10.1002/hyp.6128

Molotch, N. P., Brooks, P. D., Burns, S. P., Litvak, M., Monson, R. K., McConnell, J. R., & Musselman, K. (2009). Ecohydrological controls on snowmelt partitioning in mixed-conifer sub-alpine forests. *Ecohydrology*, *2*(2), 129–142. https://doi.org/10.1002/eco.48

Mote, P. W. (2006). Climate-driven variability and trends in mountain snowpack in western North America. *Journal of Climate*, *19*(23), 6209–6220. https://doi.org/10.1175/JCLI3971.1

Nichols, D. J., & Bryant, B. (1990). *Geologic map of the Salt Lake City 30’ x 60’ Quadrangle, north-central Utah, and Uinta County, Wyoming* (USGS Numbered Series No. 1944). Retrieved from http://pubs.er.usgs.gov/publication/i1944

Nijssen, B., O’Donnell, G. M., Hamlet, A. F., & Lettenmaier, D. P. (2001). Hydrologic sensitivity of global rivers to climate change. *Climatic Change*, *50*(1–2), 143–175. https://doi.org/10.1023/A:1010616428763

NRCS National Water and Climate Center. (2017). *SNOTEL* (SNOTEL Data & Products). Retrieved from https://www.wcc.nrcs.usda.gov/snow/

Oki, T., & Kanae, S. (2006). Global hydrological cycles and world water resources. *Science*, *313*(5790), 1068–1072. https://doi.org/10.1126/science.1128845

Peel, M. C. (2009). Hydrology: Catchment vegetation and runoff. *Progress in Physical Geography*, *33*(6), 837–844. https://doi.org/10.1177/0309133309350122

Penman, H. L. (1948). Natural evaporation from open water, bare soil and grass. *Proceedings of the Royal Society of London. Series A, Mathematical and Physical Sciences*, *193*(1032), 120–145.

Peralta-Tapia, A., Sponseller, R. A., Ågren, A., Tetzlaff, D., Soulsby, C., & Laudon, H. (2015). Scale-dependent groundwater contributions influence patterns of winter baseflow stream chemistry in boreal catchments. *Journal of Geophysical Research: Biogeosciences*, *120*(5), 2014JG002878. https://doi.org/10.1002/2014JG002878

Potter, N. J., & Zhang, L. (2007). Water balance variability at the interstorm timescale. *Water Resources Research*, *43*(5), W05405. https://doi.org/10.1029/2006WR005276

Pourmokhtarian, A., Driscoll, C. T., Campbell, J. L., Hayhoe, K., Stoner, A. M. K., Adams, M. B., … Shanley, J. B. (2017). Modeled ecohydrological responses to climate change at seven small watersheds in the northeastern United States. *Global Change Biology*, *23*(2), 840–856. https://doi.org/10.1111/gcb.13444

PRISM Climate Group. (2015). *Historical climate data, Created 1 Oct 2015*. Oregon State University. Retrieved from http://www.prism.oregonstate.edu/

Rinehart, A. J., Vivoni, E. R., & Brooks, P. D. (2008). Effects of vegetation, albedo, and solar radiation sheltering on the distribution of snow in the Valles Caldera, New Mexico. *Ecohydrology*, *1*(3), 253–270. https://doi.org/10.1002/eco.26

Scalzitti, J., Strong, C., & Kochanski, A. (2016). Climate change impact on the roles of temperature and precipitation in western U.S. snowpack variability. *Geophysical Research Letters*, *43*(10), 2016GL068798. https://doi.org/10.1002/2016GL068798

Schultz, D. M., Steenburgh, W. J., Trapp, R. J., Horel, J., Kingsmill, D. E., Dunn, L. B., … Trainor, M. (2002). Understanding Utah winter storms: The intermountain precipitation experiment. *Bulletin of the American Meteorological Society*, *83*(2), 189–210. https://doi.org/10.1175/1520-0477(2002)083<0189:UUWSTI>2.3.CO;2

Seyfried, M. S., Grant, L. E., Marks, D., Winstral, A., & McNamara, J. (2009). Simulated soil water storage effects on streamflow generation in a mountainous snowmelt environment, Idaho, USA. *Hydrological Processes*, *23*(6), 858–873. https://doi.org/10.1002/hyp.7211

Sklash, M. G., & Farvolden, R. N. (1979). The role of groundwater in storm runoff. *Journal of Hydrology*, *43*(1), 45–65. https://doi.org/10.1016/0022-1694(79)90164-1

Steenburgh, W. J., & Alcott, T. I. (2008). Secrets of the “greatest snow on earth.” *Bulletin of the American Meteorological Society, 89*(9), 1285–1293. https://doi.org/10.1175/2008BAMS2576.1

Stewart, I. T., Cayan, D. R., & Dettinger, M. D. (2004). Changes in snowmelt runoff timing in western North America under a ‘business as usual’ climate change scenario. *Climatic Change, 62*(1), 217–232.

Stewart, I. T., Cayan, D. R., & Dettinger, M. D. (2005). Changes toward earlier streamflow timing across western North America. *Journal of Climate, 18*(8), 1136–1155. https://doi.org/10.1175/JCLI3321.1

Tague, C., Grant, G., Farrell, M., Choate, J., & Jefferson, A. (2008). Deep groundwater mediates streamflow response to climate warming in the Oregon Cascades. *Climatic Change, 86*(1–2), 189–210. https://doi.org/10.1007/s10584-007-9294-8

Tennant, C. J., Crosby, B. T., & Godsey, S. E. (2015). Elevation-dependent responses of streamflow to climate warming. *Hydrological Processes, 29*(6), 991–1001. https://doi.org/10.1002/hyp.10203

Trenberth, K. E. (2011). Changes in precipitation with climate change. *Climate Research, 47*, 123–138. https://doi.org/10.3354/cr00953

Troch, P. A., Carrillo, G., Sivapalan, M., Wagener, T., & Sawicz, K. (2013). Climate-vegetation-soil interactions and long-term hydrologic partitioning: Signatures of catchment co-evolution. *Hydrologic Earth System Science, 17*(6), 2209–2217. https://doi.org/10.5194/hess-17-2209-2013

Troch, P. A., Martinez, G. F., Pauwels, V. R. N., Durcik, M., Sivapalan, M., Harman, C., … Huxman, T. (2009). Climate and vegetation water use efficiency at catchment scales. *Hydrological Processes, 23*(16), 2409–2414. https://doi.org/10.1002/hyp.7358

Trujillo, E., & Molotch, N. P. (2014). Snowpack regimes of the Western United States. *Water Resources Research, 50*(7), 5611–5623. https://doi.org/10.1002/2013WR014753

Utah Foundation. (2014). *A snapshot of 2050 - An analysis of projected population change in Utah* (No. 720). Utah Foundation. Retrieved from http://www.utahfoundation.org/uploads/rr720.pdf

Voepel, H., Ruddell, B., Schumer, R., Troch, P. A., Brooks, P. D., Neal, A., … Sivapalan, M. (2011). Quantifying the role of climate and landscape characteristics on hydrologic partitioning and vegetation response. *Water Resources Research, 47*(10), W00J09. https://doi.org/10.1029/2010WR009944

Vörösmarty, C. J., Green, P., Salisbury, J., & Lammers, R. B. (2000). Global water resources: Vulnerability from climate change and population growth. *Science*, *289*(5477), 284–288. https://doi.org/10.1126/science.289.5477.284

Vrac, M., Stein, M. L., Hayhoe, K., & Liang, X.-Z. (2007). A general method for validating statistical downscaling methods under future climate change. *Geophysical Research Letters*, *34*(18), L18701. https://doi.org/10.1029/2007GL030295

Weaver, J. E., & Mogensen, A. (1919). Relative transpiration of coniferous and broad-leaved trees in autumn and winter. *Botanical Gazette*, *68*(6), 393–424. https://doi.org/10.1086/332580

Western Regional Climate Center. (2017). *Climate summaries*. Reno, NV. Retrieved from https://wrcc.dri.edu/

Western Water Assessment. (2017). Retrieved July 21, 2017, from http://wwa.colorado.edu/climate/index.html

Wieczorek, G. F., Lips, E. W., & Ellen, S. D. (1989). Debris flows and hyperconcentrated floods along the Wasatch Front, Utah, 1983 and 1984. *Environmental and Engineering Geoscience*, *xxvi*(2), 191–208. https://doi.org/10.2113/gseegeosci.xxvi.2.191

Williams, M. W., & Melack, J. M. (1991). Solute chemistry of snowmelt and runoff in an Alpine Basin, Sierra Nevada. *Water Resources Research*, *27*(7), 1575–1588. https://doi.org/10.1029/90WR02774

Winter, T. C. (2007). The role of ground water in generating streamflow in headwater areas and in maintaining base flow. *Journal of the American Water Resources Association*, *43*(1), 15–25. https://doi.org/10.1111/j.1752-1688.2007.00003.x

Winter, T. C., Harvey, J. W., Franke, O. L., & Alley, W. M. (1998). *Ground water and surface water: A single resource* (USGS Circular No. 1139). DIANE Publishing Inc.

Wise, E. K. (2012). Hydroclimatology of the US Intermountain West. *Progress in Physical Geography*, *36*(4), 458–479. https://doi.org/10.1177/0309133312446538

Wittenberg, H., & Sivapalan, M. (1999). Watershed groundwater balance estimation using streamflow recession analysis and baseflow separation. *Journal of Hydrology*, *219*(1), 20–33. https://doi.org/10.1016/S0022-1694(99)00040-2

Wolock, D. M., & McCabe, G. J. (1999). Estimates of runoff using water-balance and atmospheric general circulation models. *JAWRA Journal of the American Water Resources Association*, *35*(6), 1341–1350. https://doi.org/10.1111/j.1752-1688.1999.tb04219.x

Xiao, X., Horton, R., Sauer, T. J., Heitman, J. L., & Ren, T. (2011). Cumulative soil water evaporation as a function of depth and time. *Vadose Zone Journal*. Retrieved from http://agris.fao.org/agris-search/search.do?recordID=US201301956925

Yaseef, N. R., Yakir, D., Rotenberg, E., Schiller, G., & Cohen, S. (2010). Ecohydrology of a semi-arid forest: Partitioning among water balance components and its implications for predicted precipitation changes. *Ecohydrology*, *3*(2), 143–154. https://doi.org/10.1002/eco.65

Yigzaw, W., & Hossain, F. (2016). Water sustainability of large cities in the United States from the perspectives of population increase, anthropogenic activities, and climate change. *Earth's Future*, *4*(12), 603–617. https://doi.org/10.1002/2016EF000393

Zapata-Rios, X., Brooks, P. D., Troch, P. A., McIntosh, J., & Guo, Q. (2015). Influence of terrain aspect on water partitioning, vegetation structure and vegetation greening in high-elevation catchments in northern New Mexico. *Ecohydrology*, 782–795. https://doi.org/10.1002/eco.1674

Zhang, C., Ding, W., Li, Y., Tang, Y., & Wang, D. (2016). Catchments' hedging strategy on evapotranspiration for climatic variability. *Water Resources Research*, *52*(11), 9036–9045. https://doi.org/10.1002/2016WR019384

Zhao, F., Zhang, L., Xu, Z., & Scott, D. F. (2010). Evaluation of methods for estimating the effects of vegetation change and climate variability on streamflow. *Water Resources Research*, *46*(3), W03505. https://doi.org/10.1029/2009WR007702

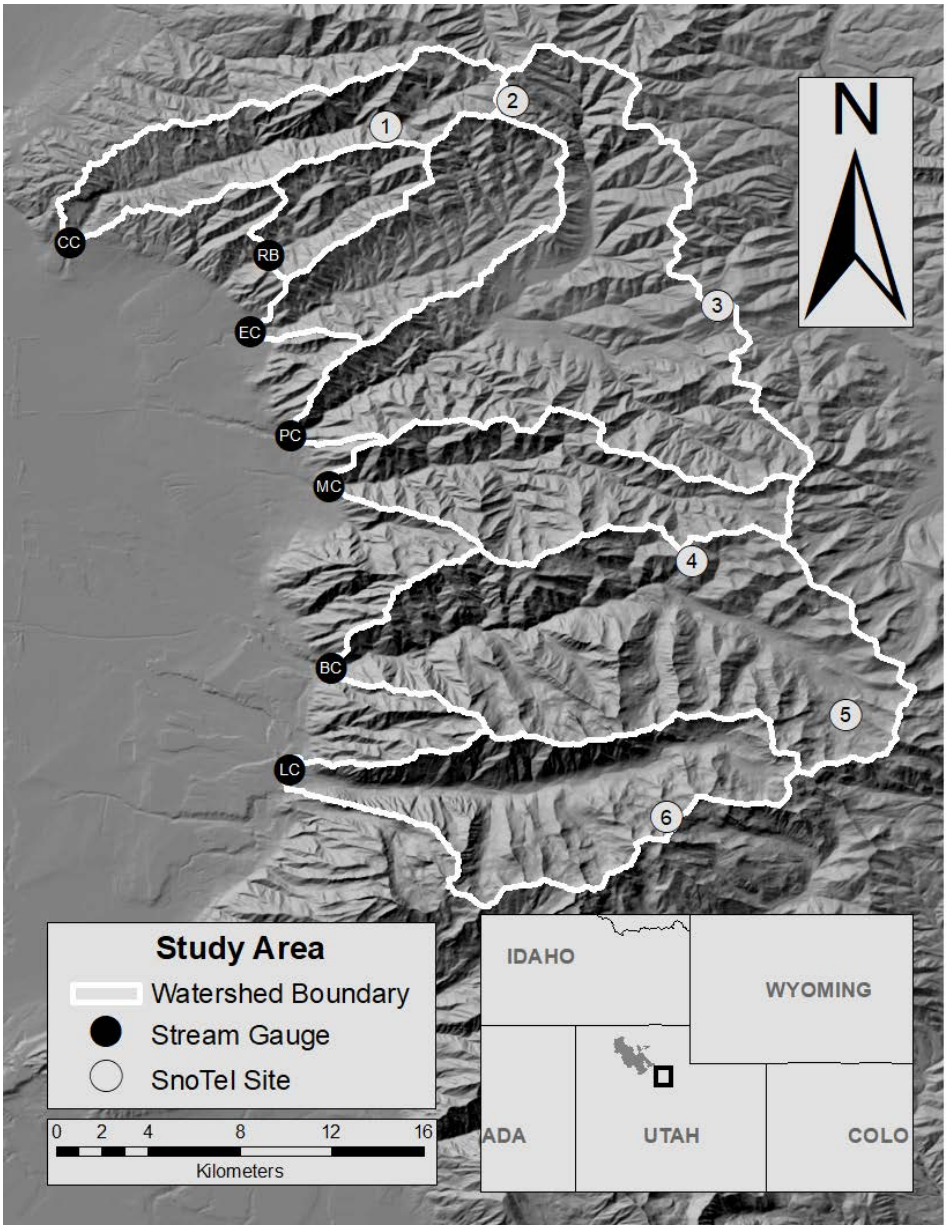

Figure 2.1. Map of Study Area in Northern Utah. These seven headwater catchments all drain from east to west but have a range of topographic, geologic, and vegetative characteristics. From north to south, the watersheds are: City (CC), Red Butte (RB), Emigration (EC), Parleys (PC), Millcreek (MC), Big Cottonwood (BC), and Little Cottonwood (LC). Six Natural Resource Conservation Service (NRCS) Snow Telemetry (SnoTel) monitoring sites exist across a range of elevations, aspects, and shading characteristics within the study area: 1) Louis Meadow, 2) Lookout Peak, 3) Parleys Summit, 4) MillD, 5) Brighton, and 6) Snowbird.

Table 2.1. Summary of Watershed Landscape Characteristics. Watersheds cover a broad range of landscapes with some similarities between certain watersheds and many differences. Mean elevation covers a range of over 1300 m. While the creeks all flow from east to west, the predominant slope aspect varies from south-facing to north-facing.

Watershed	Area (km^2)	Mean Elev (m)	Mean Slope (°)	Slope Aspect (% facing each direction)				Land Cover (% of area)				Geology
				North	East	South	West	Forest	Shrub	Desert	Rock	
CC	46	2084	23.8	23.9	15.1	39.7	21.4	41	50	5	1	Sedimentary carbonates and clastic
RB	19	2076	25.4	22.8	16.1	39.5	21.6	36	58	5	0	Sedimentary carbonates and clastic
EC	41	1963	21.0	19.6	20.4	38.4	21.6	20	66	7	1	Sedimentary carbonates and clastic
PC	135	2102	19.7	33.4	16.7	28.7	21.2	44	37	13	0	Sedimentary carbonates and clastic
MC	56	2344	27.0	36.8	14.4	27.3	21.6	69	26	1	2	Sedimentary carbonates and clastic
BC	127	2607	24.9	31.9	18.6	25.1	24.5	63	14	4	17	Metamorphic quartzite
LC	71	2698	27.1	36.5	11.5	28.8	23.2	39	16	4	38	Igneous intrusive

Table 2.2: Predictor Variables Used in a Multiple Linear Regression Analysis of Streamflow Variability. Using climate and streamflow datasets, 75 hydrologic variables are created to compare with annual streamflow variability. These variables cover over 100 years of hydrologic variability.

Metric	Period of Record	Source
Precipitation	1896 – 2014	PRISM
Annual (Oct. 1 – Sep. 30)		
Seasonal (Winter, Spring, Summer, Fall)		
Seasonal as Percent of Annual		
Monthly (12 individual months)		
Previous Year Annual (Oct. 1 – Sep. 30)		
Previous Year Seasonal (Winter, Spring, Summer, Fall)		
Temperature	1896 – 2014	PRISM
Annual (Oct. 1 – Sep. 30)		
Seasonal (Winter, Spring, Summer, Fall)		
Monthly (12 individual months)		
Previous Year Annual (Oct. 1 – Sep. 30)		
Previous Year Seasonal (Winter, Spring, Summer, Fall)		
Relative Humidity	1896 – 2014	PRISM
Annual (Oct. 1 – Sep. 30)		
Seasonal (Winter, Spring, Summer, Fall)		
Monthly (12 individual months)		
Previous Year Annual (Oct. 1 – Sep. 30)		
Previous Year Seasonal (Winter, Spring, Summer, Fall)		
Winter Baseflow	1902 – 2014	SLC Public Utilities and USGS
Snowmelt Start Date	1902 – 2014	SLC Public Utilities and USGS
Snowmelt End Date	1902 – 2014	SLC Public Utilities and USGS
Snowmelt Duration	1902 – 2014	SLC Public Utilities and USGS
Snowmelt Rate	1902 – 2014	SLC Public Utilities and USGS

Table 2.3: Hydro-climate Metrics' Central Tendency and Variability. For each metric, the mean covers a range of values throughout the seven watersheds. Climate variability around the mean is similar between all watersheds; however, streamflow variability around the mean has a much larger range, similar to snowmelt and winter baseflow metrics.

	CC	RB	EC	PC	MC	BC	LC
Annual Precipitation (mm)							
# of Years	119	119	119	119	119	119	119
Mean	846	799	791	815	921	1041	1290
Standard Deviation	176	169	166	167	188	218	274
Annual Mean Temperature (°C)							
# of Years	119	119	119	119	119	119	119
Mean	6.7	6.8	6.9	6.3	5.2	4.2	3.3
Standard Deviation	0.8	0.8	0.8	0.8	0.8	0.8	0.9
Annual Mean Relative Humidity (%)							
# of Years	119	119	119	119	119	119	119
Mean	49.5	48.9	47.9	46.9	48.9	50.4	51.2
Standard Deviation	3.1	3.0	2.8	2.8	3.4	3.7	3.7
Annual Streamflow (mm)							
# of Years	110	72	105	107	111	107	99
Mean	322	183	147	227	242	507	814
Standard Deviation	113	106	105	124	88	147	217
Annual Water Yield							
# of Years	110	72	105	107	111	107	99
Mean	0.38	0.21	0.18	0.26	0.26	0.49	0.63
Standard Deviation	0.08	0.09	0.10	0.11	0.06	0.08	0.08
Snowmelt Start Date (Day of Water Year)							
# of Years	108	48	102	104	97	109	100
Mean	168	149	159	159	173	174	187
Standard Deviation	18	16	17	17	25	14	15
Snowmelt End Date (Day of Water Year)							
# of Years	108	48	102	104	97	109	100
Mean	355	303	313	317	374	336	340
Standard Deviation	50	60	53	46	70	44	36
Snowmelt Rate (mm/day)							
# of Years	106	48	100	103	92	107	99
Mean	1.27	0.86	0.74	0.85	0.87	2.46	4.45
Standard Deviation	0.42	0.44	0.42	0.41	0.29	0.56	1.03
Winter Baseflow (mm/day)							
# of Years	111	51	110	110	105	111	102
Mean	0.41	0.25	0.12	0.19	0.38	0.51	0.53
Standard Deviation	0.08	0.08	0.07	0.06	0.12	0.15	0.12

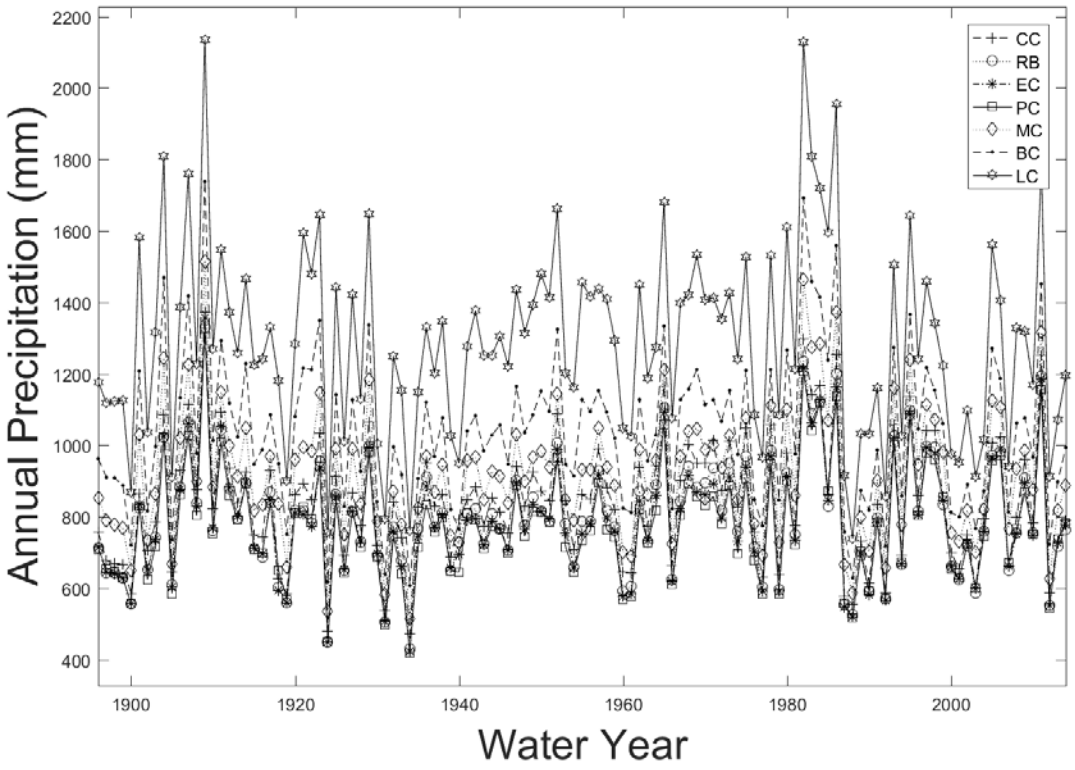

Figure 2.2. Precipitation Time Series. In the seven watersheds, annual precipitation ranges from 420 mm to 2135 mm during 1896 – 2014 with watershed means ranging from 780 to 1290 mm. All watersheds experienced annual precipitation between 740 mm and 1330 mm during the period of record. There is no significant trend in annual precipitation over time.

Table 2.4. Trends over Entire Period and Period of Greatest Warming. This table presents the amount of change over time in climatic and hydrologic variables over the entire period of record and 1964 – 2014, which was chosen because it is the period of the greatest rate of change in annual temperature. Only variables with significant ($p<0.05$) trends are presented. The significant warming trend is reflected in a drying trend in relative humidity but is not yet evident in streamflow. Two ** denotes significance at $p<0.001$; One * denotes significance at $p<0.01$; No asterisk denotes significant at $p<0.05$.

	Change Per Decade						
	CC	**RB**	**EC**	**PC**	**MC**	**BC**	**LC**
Annual Precipitation (mm)							
Entire Dataset	NA	NA	NA	NA	NA	NA	NA
1964 - 2014	NA	NA	NA	NA	NA	NA	NA
Annual Mean Temperature (°C)							
Entire Dataset	0.07**	0.07**	0.07**	0.07**	0.08**	0.07**	0.10**
1964 - 2014	0.26**	0.25**	0.20**	0.20**	0.34**	0.36**	0.40**
Annual Mean Relative Humidity (%)							
Entire Dataset	NA	NA	NA	NA	NA	NA	NA
1964 - 2014	-1.1**	-1.0**	-0.8*	-0.8*	-1.4**	-1.6**	-1.8**
Annual Streamflow (mm)							
Entire Dataset	NA	NA	NA	NA	NA	NA	NA
1964 - 2014	NA	NA	NA	NA	NA	NA	NA
Annual Water Yield							
Entire Dataset	NA	NA	NA	NA	NA	-0.0064	0.0069
1964 - 2014	NA	NA	NA	-0.022	-0.014	NA	NA
Snowmelt Start Date (days)							
Entire Dataset	NA	NA	NA	-1.1	NA	NA	NA
1964 - 2014	NA	NA	NA	NA	NA	NA	-3.4
Snowmelt End Date (days)							
Entire Dataset	-4.4*	NA	-5.1*	-4.2*	NA	-2.9	3.2*
1964 - 2014	-10	NA	NA	-13*	NA	NA	NA
Snowmelt Rate (mm/day)							
Entire Dataset	NA	NA	NA	NA	NA	NA	NA
1964 - 2014	NA	NA	NA	NA	NA	NA	NA
Winter Baseflow (mm/day)							
Entire Dataset	NA	NA	NA	NA	NA	NA	0.014**
1964 - 2014	NA	NA	NA	NA	NA	NA	NA

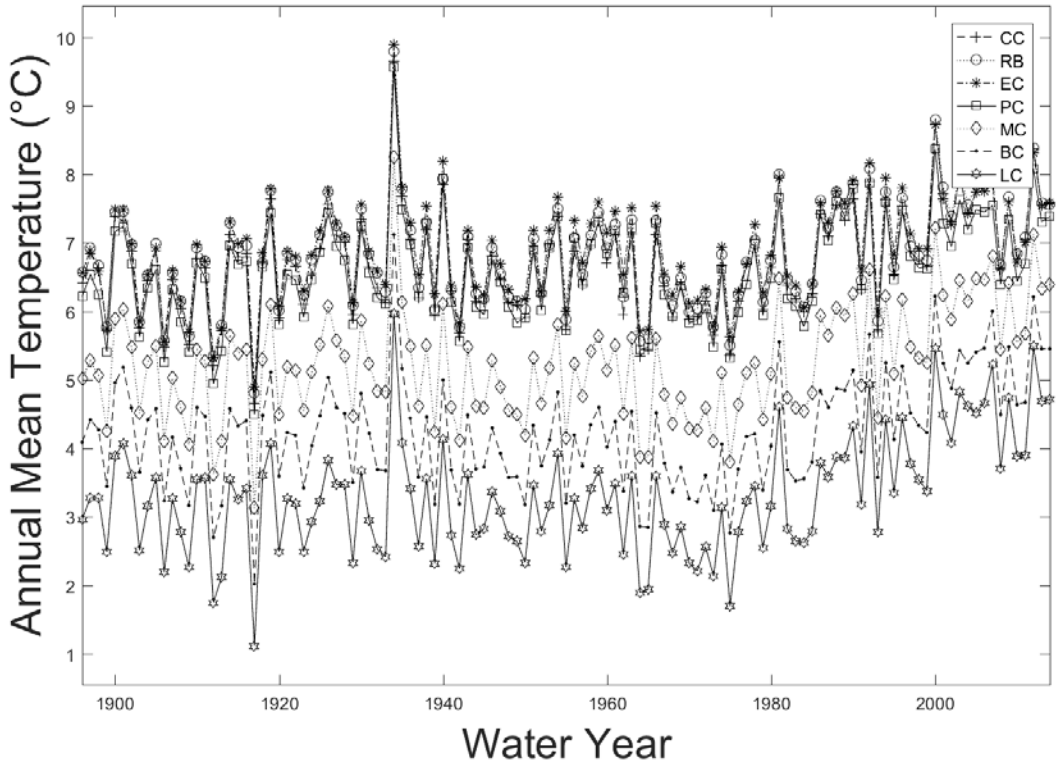

Figure 2.3. Temperature Time Series. In the seven watersheds, annual temperature ranges from 1.1°C to 9.9°C during 1896 – 2014 with watershed means ranging from 6.6°C to 3.3°C. All watersheds experienced annual temperature between 4.9° - 6.0°C during the period of record. Temperature significantly warms in each watershed, with the greatest rate of warming occurring from 1964 to 2014.

Table 2.5: Correlation of Interannual Hydro-climate Variability between Watersheds. Annual precipitation (PPT), annual temperature (T), annual relative humidity (RH), annual streamflow (Q), winter baseflow (Q Base), snowmelt rate (MR), snowmelt start day (Start), and snowmelt end day (End). Climate variability is similar between watersheds, illustrated by high Pearson R values. Streamflow variability is less correlated than climate variability. Interannual variability is least correlated for winter baseflow and snowmelt metrics as these are controlled by unique watershed landscape features.

	Pearson R							
Watersheds	**PPT**	**T**	**RH**	**Q**	**Q Base**	**MR**	**Start**	**End**
CC; RB	1.00	1.00	1.00	0.98	0.84	0.88	0.54	0.72
CC; EC	0.99	0.99	0.98	0.94	0.59	0.89	0.52	0.72
CC; PC	0.98	0.98	0.98	0.96	0.69	0.86	0.65	0.69
CC; MC	0.98	0.99	0.99	0.93	0.71	0.82	0.49	0.66
CC; BC	0.95	0.98	0.97	0.90	0.63	0.72	0.51	0.70
CC; LC	0.93	0.96	0.93	0.89	0.54	0.72	0.35	0.48
RB; EC	1.00	0.99	0.99	0.97	0.76	0.93	0.70	0.70
RB; PC	0.99	0.99	0.99	0.96	0.83	0.94	0.59	0.75
RB; MC	0.98	0.99	0.98	0.93	0.84	0.82	0.48	0.68
RB; BC	0.95	0.97	0.97	0.92	0.85	0.81	0.23	0.79
RB; LC	0.93	0.95	0.92	0.88	0.68	0.80	0.18	0.61
EC; PC	1.00	1.00	1.00	0.94	0.54	0.90	0.63	0.69
EC; MC	0.98	0.97	0.97	0.89	0.49	0.77	0.32	0.57
EC; BC	0.95	0.95	0.94	0.88	0.55	0.74	0.20	0.66
EC; LC	0.93	0.93	0.90	0.83	0.42	0.69	0.16	0.43
PC; MC	0.99	0.97	0.97	0.93	0.70	0.82	0.39	0.61
PC; BC	0.96	0.95	0.94	0.91	0.74	0.77	0.48	0.68
PC; LC	0.93	0.93	0.90	0.88	0.69	0.68	0.28	0.42
MC; BC	0.99	0.99	0.99	0.89	0.76	0.76	0.28	0.56
MC; LC	0.97	0.98	0.97	0.83	0.52	0.67	0.13	0.45
BC; LC	0.99	0.99	0.98	0.87	0.66	0.68	0.47	0.49
Minimum	0.93	0.93	0.90	0.83	0.42	0.67	0.13	0.42
Mean	0.97	0.97	0.96	0.91	0.67	0.79	0.41	0.62
Maximum	1.00	1.00	1.00	0.98	0.85	0.94	0.70	0.79

Table 2.6: Climate Means and Elevation. A linear regression analysis of mean watershed climate gradients with respect to watershed elevation shows a strong correlation for both annual precipitation and temperature, and a weaker correlation for relative humidity. The correlation between precipitation and elevation is expected as a result of orographic uplift. The correlation between temperature and elevation is similar to a typical moist adiabatic lapse rate.

	Correlation with elevation
Annual Precipitation	
Slope (mm/km)	602
R^2	0.84
p Value	>0.01
Annual Temperature	
Slope (°C/km)	-4.98
R^2	0.97
p Value	>0.001
Annual Relative Humidity	
Slope (%/km)	4.11
R^2	0.60
p Value	0.025

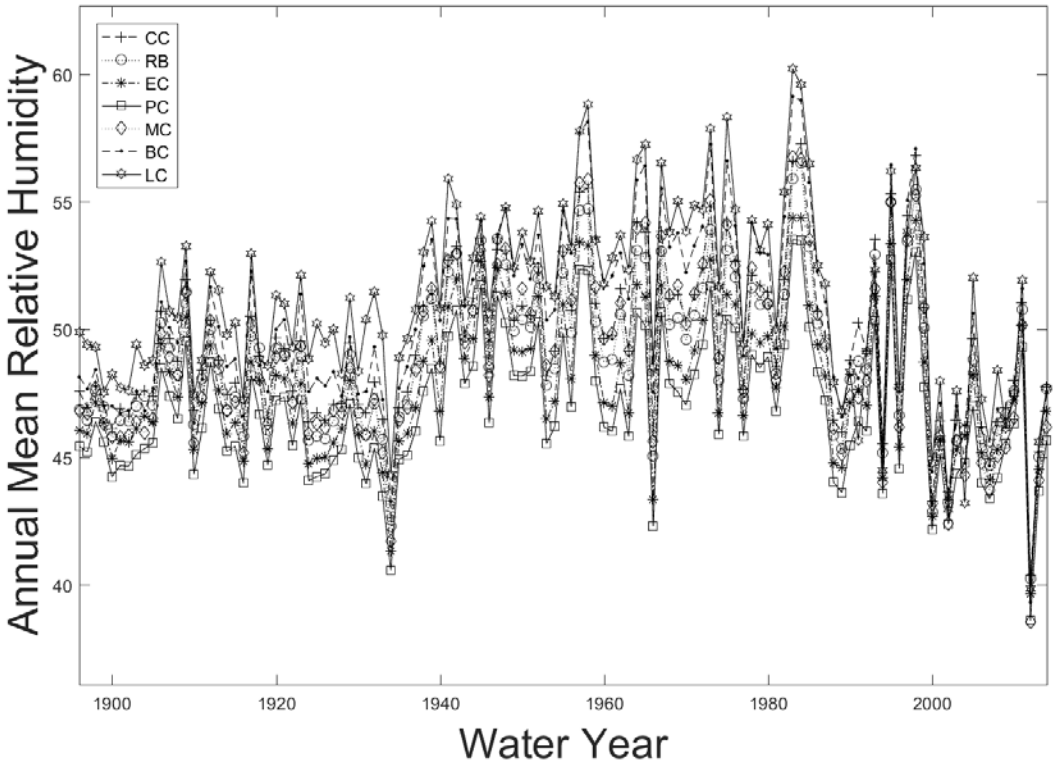

Figure 2.4. Relative Humidity. In the seven watersheds, annual mean relative humidity ranges from 39% to 60% during 1896 – 2014 with watershed means ranging from 47% to 51%. All watersheds experienced annual mean relative humidity between 40% and 53% during the period of record. No trend in relative humidity exists over the entire period of record ($p>0.05$). However, during the period of the greater rate of warming (1964 – 2014), relative humidity decreases significantly in every watershed with rates ranging from -0.8% to -1.8% / decade in PC and LC, respectively ($p<0.01$).

Table 2.7. Seasonal Climate Metrics Means and Variability. Fall (Sep., Oct., and Nov.) winter (Dec., Jan., Feb.), spring (Mar., Apr., May), and summer (Jun., Jul., Aug.) climate generally follow spatial and interannual temporal patterns that are similar to annual climate patterns. The majority of precipitation falls during the coldest seasons (winter and spring), while the hottest season, summer, is typically also the driest.

	CC	RB	EC	PC	MC	BC	LC
Fall Precipitation (mm)							
Mean	188	182	182	182	203	223	288
Standard Deviation	70	68	67	67	76	84	112
Winter Precipitation (mm)							
Mean	299	271	269	260	318	374	479
Standard Deviation	102	95	94	89	106	130	165
Spring Precipitation (mm)							
Mean	272	257	252	248	300	334	397
Standard Deviation	86	82	79	77	93	106	129
Summer Precipitation (mm)							
Mean	87	88	89	91	100	110	127
Standard Deviation	44	44	44	44	47	50	57
Mean Fall Temperature (°C)							
Mean	7.3	7.4	7.6	7.3	6.0	5.0	4.1
Standard Deviation	1.1	1.1	1.1	1.1	1.1	1.1	1.1
Mean Winter Temperature (°C)							
Mean	-3.0	-2.9	-3.0	-3.2	-4.1	-4.8	-5.5
Standard Deviation	1.4	1.4	1.4	1.4	1.4	1.4	1.5
Mean Spring Temperature (°C)							
Mean	5.2	5.3	5.4	5.0	3.3	2.1	1.0
Standard Deviation	1.4	1.4	1.4	1.4	1.4	1.4	1.4
Mean Summer Temperature (°C)							
Mean	17.3	17.4	17.6	17.3	15.7	14.7	13.6
Standard Deviation	1.1	1.1	1.0	1.1	1.1	1.1	1.1
Mean Fall Relative Humidity (%)							
Mean	47.5	46.6	45.4	45.4	48.3	49.5	50.4
Standard Deviation	4.7	4.6	4.2	4.3	5.1	5.5	5.5
Mean Winter Relative Humidity (%)							
Mean	65.4	65.0	63.6	61.8	62.8	63.1	64.3
Standard Deviation	3.8	3.8	3.5	3.4	4.3	4.6	4.8
Mean Spring Relative Humidity (%)							
Mean	48.7	48.1	47.1	46.0	47.7	49.4	49.8
Standard Deviation	4.5	4.4	4.2	4.1	4.8	5.1	5.2
Mean Summer Relative Humidity (%)							
Mean	36.4	35.9	35.2	34.5	37.0	39.7	40.1
Standard Deviation	4.2	4.1	4.0	3.9	4.5	4.9	4.8

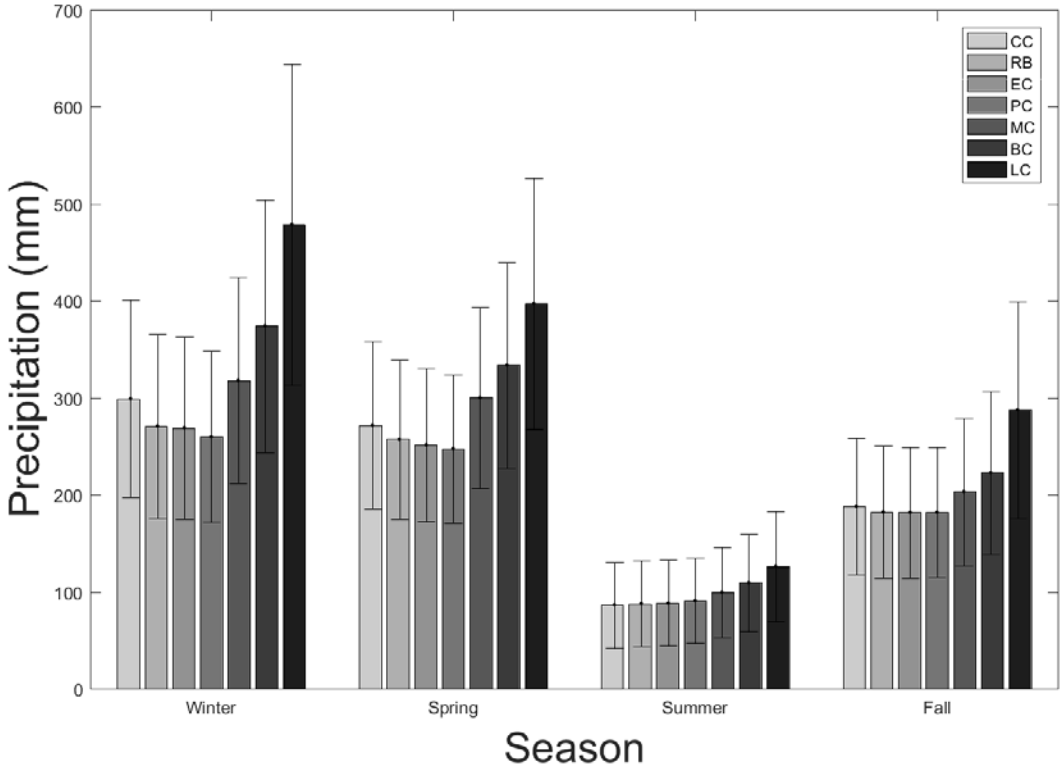

Figure 2.5. Seasonal Precipitation. Most precipitation occurs during the winter and spring seasons. Summer is the driest season. Fall accounts for nearly 25% of annual precipitation. Error bars indicate one standard deviation from the mean seasonal value, indicating similar interannual variability in precipitation between watersheds.

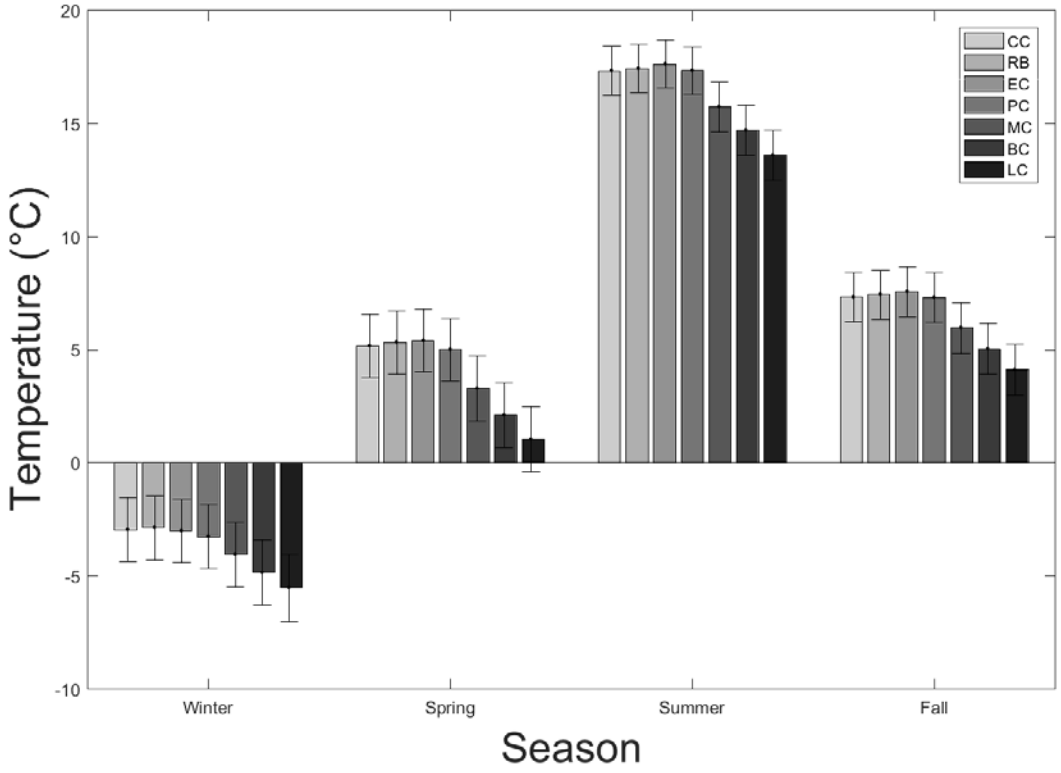

Figure 2.6. Seasonal Temperature. Mean winter temperature is below freezing in every watershed. Temperature peaks during the summer season and is transitional during the spring and fall. Error bars indicate one standard deviation from the mean seasonal value, indicating nearly identical interannual variability in temperature between watersheds.

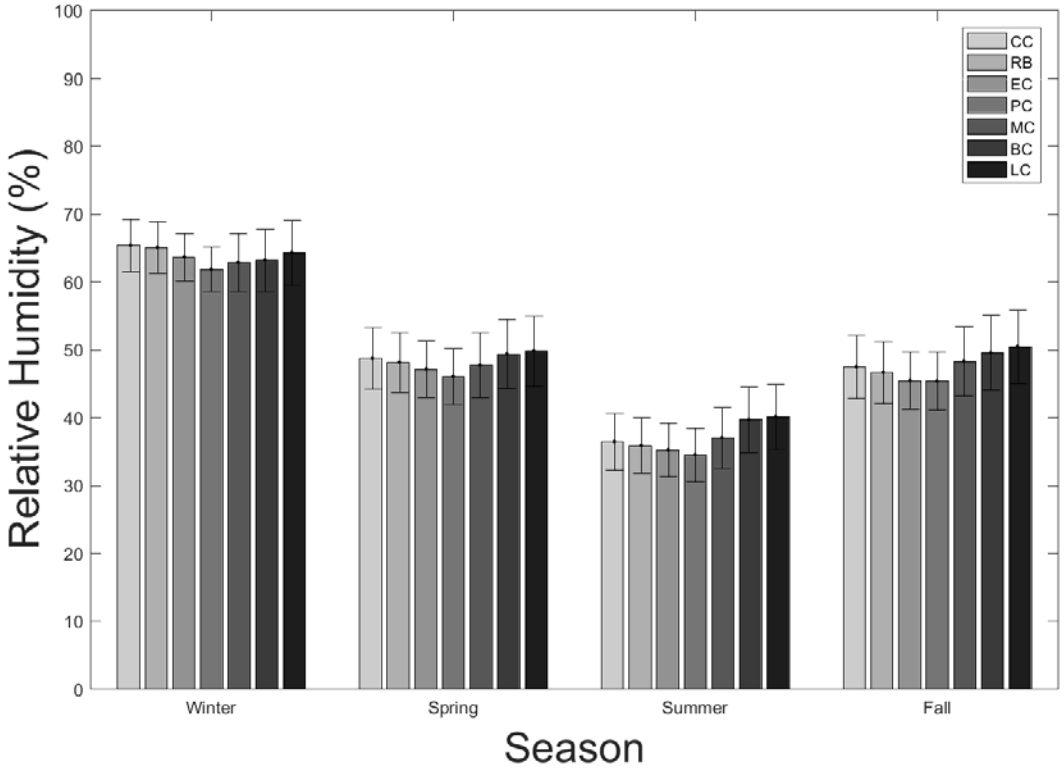

Figure 2.7. Seasonal Relative Humidity. Relative humidity peaks during the winter and is a minimum during the summer. Error bars indicate one standard deviation from the mean seasonal value, indicating nearly identical interannual variability in relative humidity between watersheds.

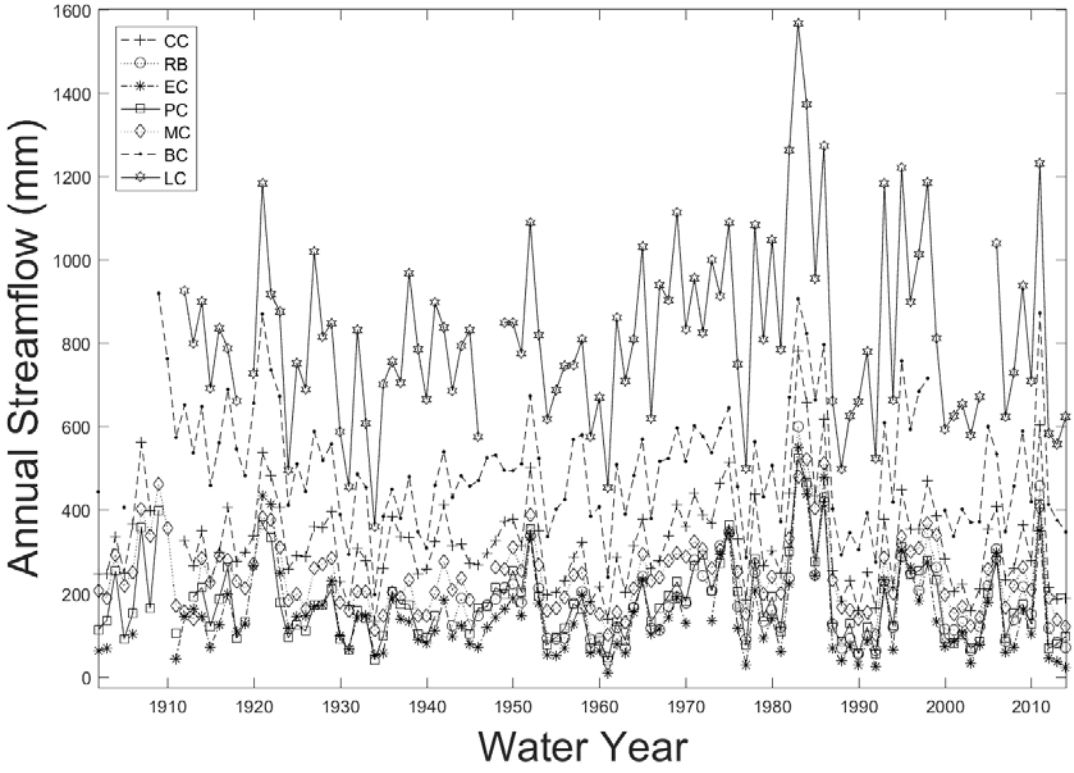

Figure 2.8. Streamflow Time Series. In the seven watersheds, mean annual streamflow, normalized by watershed area, ranges from 7 mm to 1568 mm during 1896 – 2014 with watershed means ranging from 147 to 814 mm. There is no significant trend in annual streamflow over time.

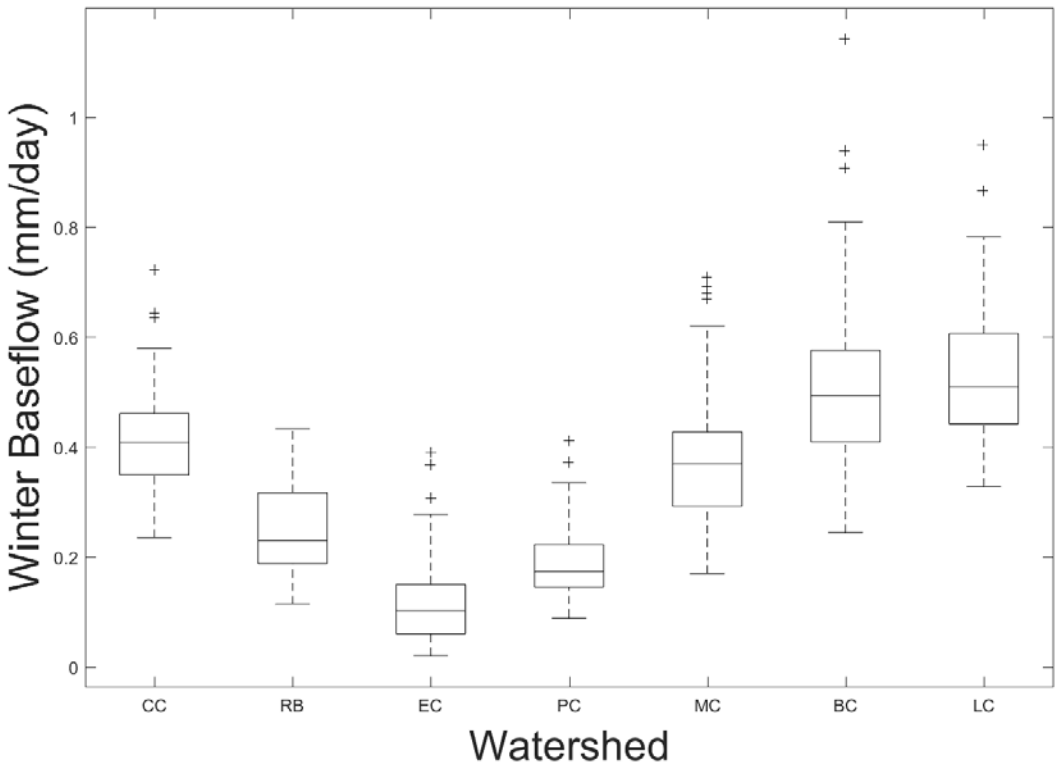

Figure 2.9. Winter Baseflow Variability in the Seven Watersheds. Box and whisker plots present the range of median values from 0.12 mm/day to 0.53 mm/day during 1896 – 2014. There is a significant amount of interannual variability in winter baseflow in each watershed.

Table 2.8. Winter Baseflow Intra-annual Variability. The standard error of mean winter baseflow represents the daily variability of streamflow during December and January within a given year. The low range of standard error values indicates that streamflow is relatively stable during these months. This signifies that the main influence on streamflow during these months comes from water stored in the subsurface rather than incoming precipitation, which mainly adds to the snowpack at this time. The values of the standard error of the mean are substantially lower than the interannual variability of winter baseflow.

	Standard Error of Mean December - January Streamflow (mm/day)						
1902 - 2014	**CC**	**RB**	**EC**	**PC**	**MC**	**BC**	**LC**
Minimum	1.0E-03	8.3E-04	1.8E-18	5.6E-04	1.3E-03	2.4E-03	2.6E-03
Mean	3.7E-03	3.9E-03	3.7E-03	4.0E-03	9.4E-03	7.6E-03	8.6E-03
Maximum	1.3E-02	1.9E-02	2.2E-02	2.2E-02	5.8E-02	2.7E-02	3.2E-02

Table 2.9: Multiple Linear Regression of Winter Baseflow Predictors. Precipitation, snowmelt, and winter baseflow from the Previous Year (PY) add predictability to winter baseflow variability. Factors that were included in the regression analysis but did not add predictability include: the previous year's annual and seasonal temperature, the start and end date of snowmelt, and all precipitation, temperature, and snowmelt variables from 2-4 years prior to the winter baseflow.

	PY Sept & Oct Precipitation (mm)	PY Annual Precipitation (mm)	PY Snowmelt Rate (mm/day)	PY Snowmelt Duration (days)	PY Baseflow (mm/day)	Remaining Error
City Creek						
Estimate		1.1E-04	0.104			
Predictability Added (%)		34.9	15.4			49.7
Red Butte						
Estimate	2.3E-04	8.3E-05	0.097			
Predictability Added (%)	15.1	37.5	13.6			33.8
Emigration						
Estimate		-5.5E-05	-0.006	8.7E-04	0.496	
Predictability Added (%)		16.0	12.1	19.1	17.0	35.7
Parleys						
Estimate	4.4E-04	7.5E-05	0.066			
Predictability Added (%)	12.8	21.3	8.4			57.5
Millcreek						
Estimate		1.8E-04	0.220			
Predictability Added (%)		38.4	16.7			44.8
Big Cottonwood						
Estimate	7.7E-04	-5.1E-05	0.14	1.1E-03		
Predictability Added (%)	11.1	32.5	8.6	5.7		42.1
Little Cottonwood						
Estimate	6.2E-04	1.5E-05		1.1E-03	0.39	
Predictability Added (%)	34.9	8.8		5.7	11.5	39.1

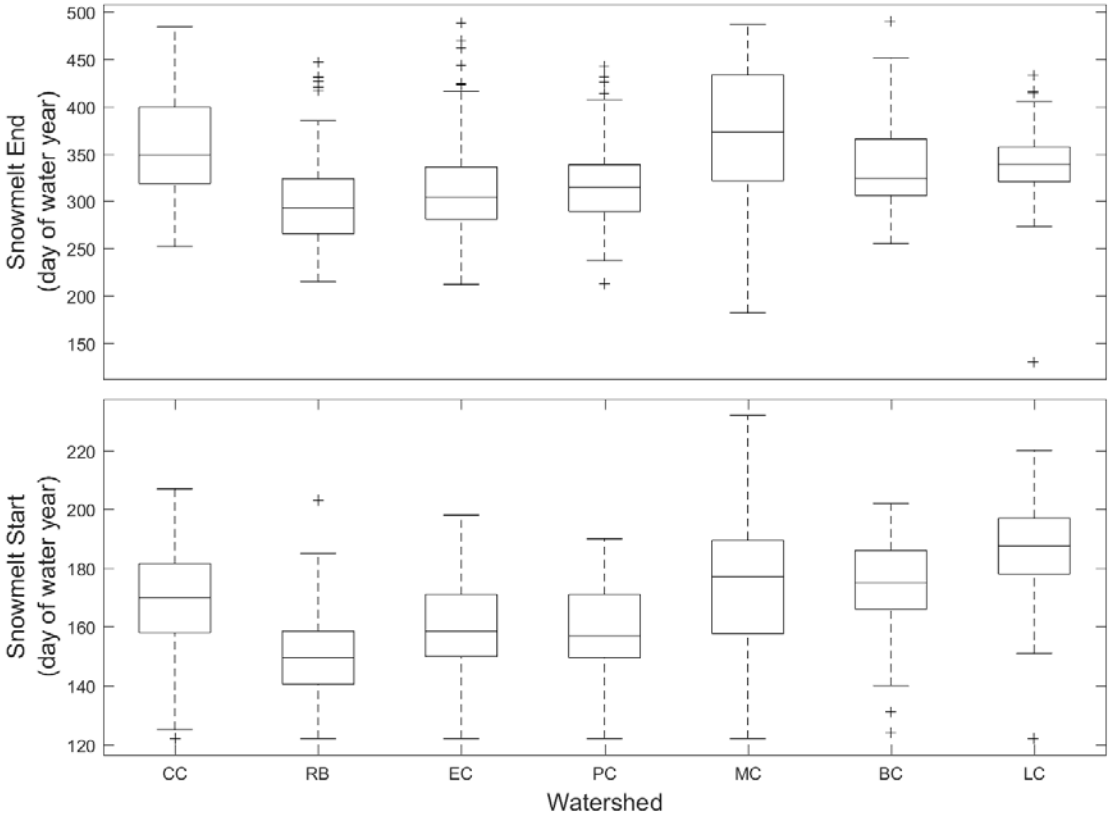

Figure 2.10. Snowmelt Timing. Day of water year values correspond to the number of days after October 1, the start of the water year. When the end of snowmelt occurs after the start of the next water year, the end date of snowmelt continues to reference the year snowmelt began, allowing for values greater than 365. Snowmelt start date typically ranges from February 26, in RB to April 5 in LC. Snowmelt end date typically ranges from July 30 in RB to October 9 in MC. Snowmelt start and end dates are used to calculate the snowmelt duration.

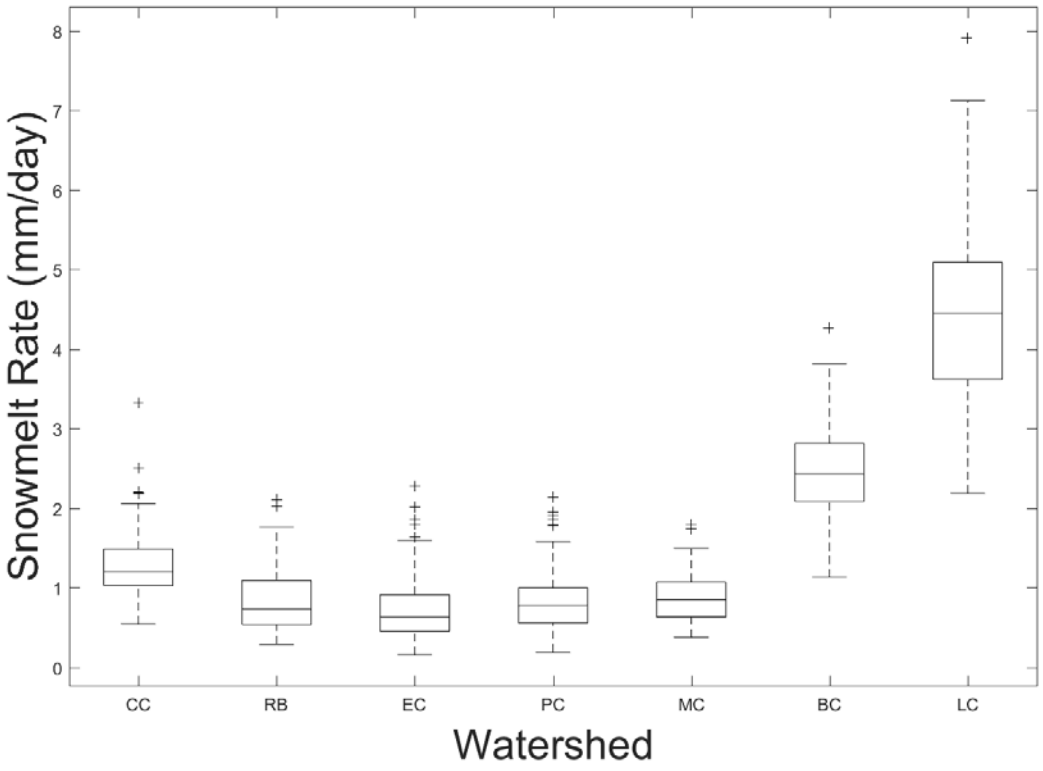

Figure 2.11. Snowmelt Rate Interannual Variability. Snowmelt rate is calculated as the amount of snowmelt divided by the snowmelt duration. Snowmelt rate ranges from 0.15 in EC to 7.92 in LC. There is significant interannual variability in snowmelt rate within each watershed.

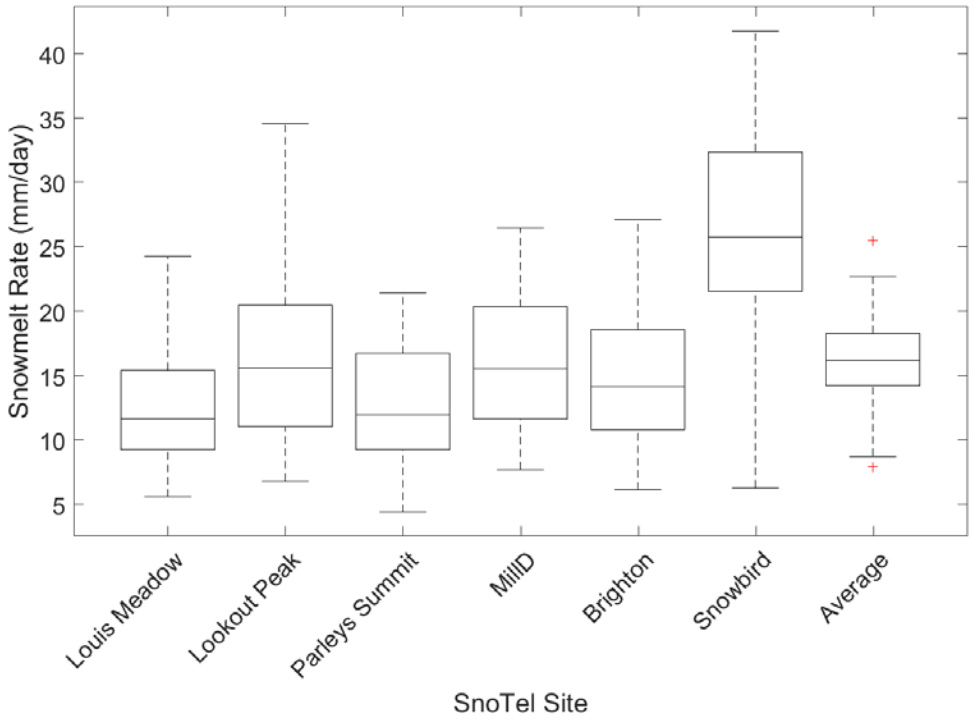

Figure 2.12: SnoTel-derived Snowmelt Rate. Six different SnoTel sites are within the watershed boundaries. A seventh data series is calculated as the mean of the six SnoTel sites. SnoTel sites are arranged here from north (left) to south (right). Five of the six SnoTel sites, all except Snowbird, have statistically similar mean snowmelt rates.

Table 2.10: Regression Model of SnoTel Snowmelt Rate and Watershed Snowmelt Rate. Snowmelt rate from six SnoTel sites, as well as the average of all six sites, is correlated to the hydrograph-derived watershed snowmelt rate in each of the seven watersheds. SnoTel snowmelt rate is generally an order of magnitude greater than the watershed snowmelt rate. In six of the seven watersheds (all except MC), the average snowmelt rate from all six SnoTel sites explains the most variability in the watershed snowmelt rate. In MC, the Louis Meadow SnoTel site explains the most variability.

	CC	**RB**	**EC**	**PC**	**MC**	**BC**	**LC**
Louis Meadow							
Coefficient	0.04	0.05	0.05	0.06	0.03	0.06	0.09
R^2	0.23	0.27	0.28	0.27	0.58	0.15	0.17
p Value	4.0E-02	2.7E-02	3.0E-02	3.4E-02	6.4E-03	8.4E-02	8.0E-02
Lookout Peak							
Coefficient	0.03	0.05	0.05	0.05	0.01	0.07	0.06
R^2	0.15	0.27	0.21	0.29	0.01	0.26	0.06
p Value	8.5E-02	2.7E-02	5.9E-02	2.8E-02	3.2E-01	2.9E-02	1.9E-01
Parley's Summit							
Coefficient	0.03	0.04	0.04	0.08	0.03	0.04	0.12
R^2	0.01	0.09	0.06	0.29	0.18	0.00	0.22
p Value	3.0E-01	1.4E-01	2.1E-01	2.7E-02	1.2E-01	3.6E-01	5.3E-02
Mill D							
Coefficient	0.05	0.07	0.06	0.07	0.03	0.10	0.10
R^2	0.30	0.34	0.28	0.31	0.29	0.36	0.17
p Value	2.0E-02	1.3E-02	2.9E-02	2.2E-02	6.2E-02	1.1E-02	7.7E-02
Brighton							
Coefficient	0.05	0.06	0.06	0.06	0.03	0.08	0.10
R^2	0.24	0.24	0.16	0.19	0.11	0.19	0.14
p Value	3.8E-02	3.5E-02	8.6E-02	6.7E-02	1.8E-01	5.7E-02	1.0E-01
Snowbird							
Coefficient	0.03	0.03	0.03	0.04	0.00	0.05	0.09
R^2	0.18	0.22	0.19	0.15	0.00	0.27	0.35
p Value	6.6E-02	4.5E-02	6.7E-02	9.6E-02	8.0E-01	2.8E-02	1.5E-02
Average							
Coefficient	0.08	0.10	0.10	0.11	0.05	0.13	0.17
R^2	0.43	0.56	0.51	0.52	0.46	0.48	0.41
p Value	4.6E-03	8.6E-04	2.6E-03	2.2E-03	1.9E-02	2.6E-03	8.1E-03

Table 2.11. Snowmelt Correlation Residuals and Snowmelt Variables. SnoTel snowmelt rate and watershed snowmelt rate correlation residual values are significantly ($p<0.05$) and positively correlated to the SnoTel snowmelt duration.

	CC	RB	EC	PC	MC	BC	LC
Hydrograph Melt Amount (mm)							
Coefficient	1.1E-03	1.7E-03	1.7E-03	2.2E-03	7.3E-04	1.5E-03	1.5E-03
R^2	0.19	0.29	0.22	0.27	0.06	0.16	0.19
p Value	5.8E-02	2.3E-02	5.3E-02	3.4E-02	2.5E-01	8.0E-02	6.7E-02
Hydrograph Melt Duration (days)							
Coefficient	1.0E-03	2.1E-03	6.8E-04	4.7E-04	3.1E-04	-3.3E-03	-2.6E-04
R^2	0.00	0.00	0.00	0.00	0.00	0.00	0.00
p Value	4.9E-01	3.3E-01	6.9E-01	8.7E-01	6.3E-01	4.2E-01	9.7E-01
SnoTel Melt Amount (mm)							
Coefficient	5.8E-04	7.3E-04	7.4E-04	8.2E-04	4.3E-04	7.1E-04	1.6E-03
R^2	0.11	0.18	0.17	0.18	0.19	0.03	0.18
p Value	1.3E-01	6.5E-02	7.8E-02	7.0E-02	1.2E-01	2.4E-01	7.6E-02
SnoTel Melt Duration (days)							
Coefficient	2.5E-02	3.5E-02	3.2E-02	3.8E-02	1.2E-02	3.7E-02	7.8E-02
R^2	0.31	0.56	0.48	0.56	0.32	0.25	0.60
p Value	1.9E-02	7.6E-04	3.6E-03	1.3E-03	5.0E-02	3.3E-02	7.3E-04

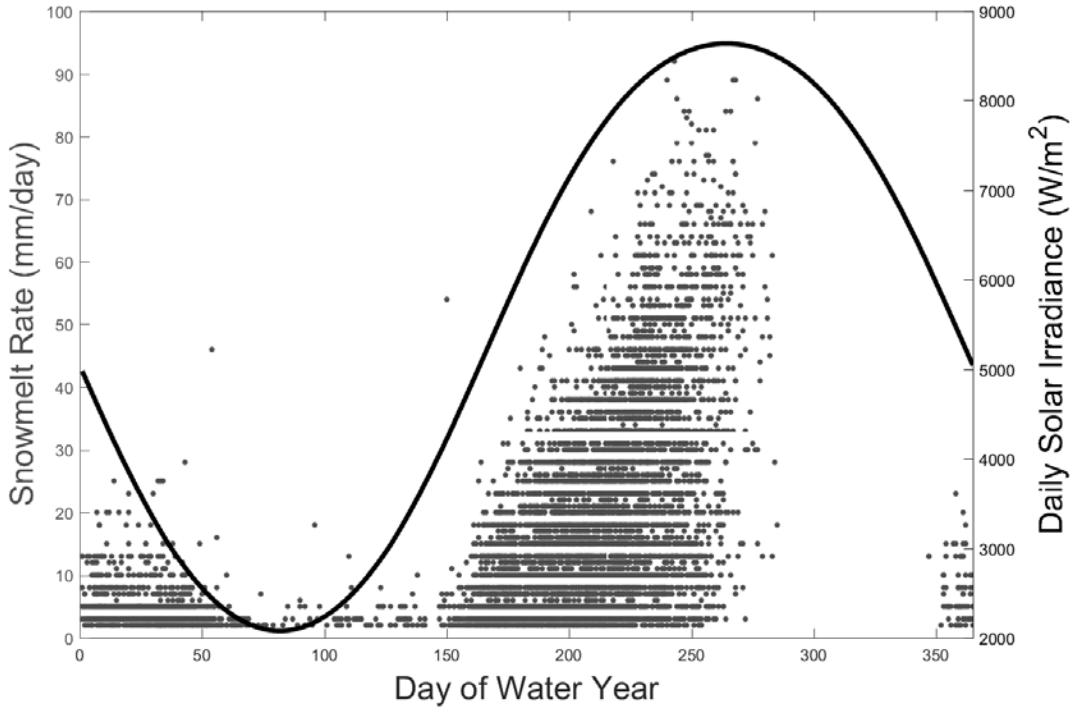

Figure 2.13. SnoTel Snowmelt Rate and Solar Radiation. Snowmelt rate follows a similar annual pattern as the incoming solar radiation. Maximum snowmelt rate decreases from the start of the snow season in late September until December and then increases from approximately March 1 until the snowpack completely ablates.

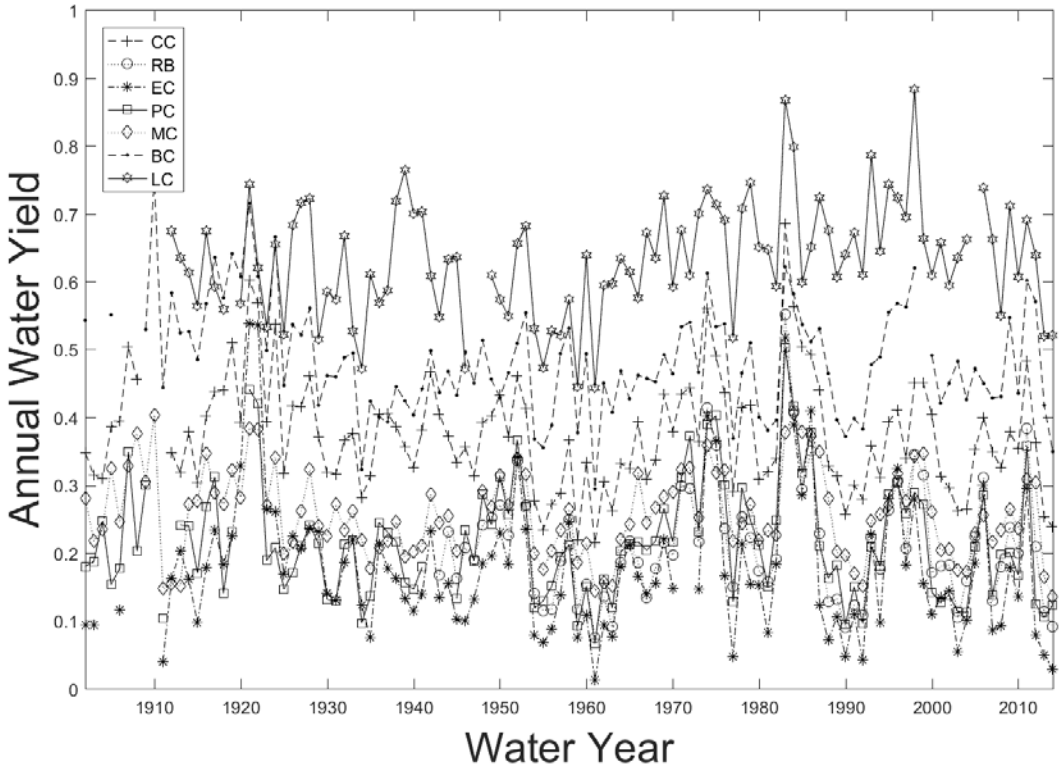

Figure 2.14. Water Yield Time Series. Annual water yield is defined as the fraction of annual precipitation that is partitioned to annual streamflow, with typical values ranging from 0 to 1. Throughout the period of record, the water yield is different between watersheds. The significant variability of water yield within and between watersheds indicates that nearly any fraction of precipitation may be partitioned to streamflow during any given year.

Table 2.12: Water Yield and Landscape Correlation. Linear regression analysis of watershed mean annual water yield predicted by landscape characteristics indicates that only elevation and rock land cover significantly correlate ($p < 0.01$) to watershed mean water yield. Water yield increases as both elevation and the fractional rock area increase.

	Regression Slope	**R^2**	**P-Value**
Elevation (m)	5.17E-04	0.73	9.32E-03
Slope Steepness (°)	3.34E-02	0.18	1.89E-01
North-Facing Aspect (%)	1.2	0.10	2.51E-01
East-Facing Aspect (%)	-3.3	0.17	1.93E-01
South-Facing Aspect (%)	-1.2	0.04	3.19E-01
West-Facing Aspect (%)	10.6	0.49	4.75E-02
Forest Land Cover (%)	2.48E-03	0.00	5.99E-01
Shrub Land Cover (%)	-6.12E-03	0.46	5.60E-02
Desert Land Cover (%)	-1.69E-02	0.00	4.12E-01
Rock Land Cover (%)	1.08E-02	0.82	3.24E-03

Table 2.13: Hydrologic Partitioning Metrics' Central Tendency and Variability. For each metric, the mean and standard deviation cover a range of values throughout the seven watersheds.

	CC	RB	EC	PC	MC	BC	LC
Annual Evapotranspiration (mm)							
# of Years	110	72	105	107	111	107	99
Mean	525	635	642	609	684	532	468
Standard Deviation	109	108	119	109	139	128	137
Annual Stormflow (mm)							
# of Years	110	51	105	107	111	107	99
Mean	38	25	24	29	28	87	159
Standard Deviation	20	21	19	19	13	29	50
Annual Baseflow (mm)							
# of Years	110	51	105	107	111	107	99
Mean	284	171	123	149	215	420	654
Standard Deviation	95	97	87	79	77	120	172
Annual Wetting (mm)							
# of Years	110	51	105	107	111	107	99
Mean	808	807	765	758	899	952	1122
Standard Deviation	155	173	146	151	180	195	224
Annual Horton Index							
# of Years	110	51	105	107	111	107	99
Mean	0.65	0.80	0.85	0.81	0.76	0.56	0.42
Standard Deviation	0.08	0.09	0.09	0.08	0.06	0.08	0.09

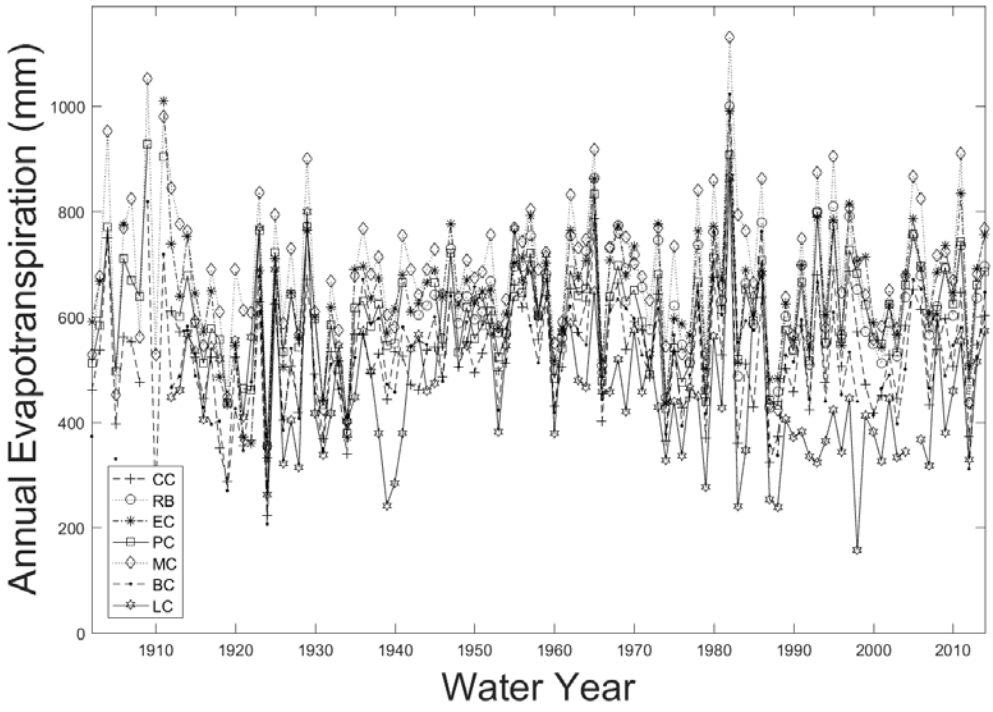

Figure 2.15. Evapotranspiration Time Series. In the seven watersheds, annual evapotranspiration ranges from 157 mm to 1132 mm during 1902 – 2014 with watershed means ranging from 470 mm to 680 mm. There is no significant trend in annual evapotranspiration over time, except for a decrease of -11mm / decade in LC that is significant ($p = 0.017$) during the entire period of record, but not significant during the period of greatest warming (1964 – 2014).

Table 2.14: Correlation of Interannual Hydrologic Partitioning Variability between Watersheds. Annual evapotranspiration (ET), annual stormflow (S), annual baseflow (U), annual Horton Index (HI), and Normalized Differential Vegetation Index (NDVI). Wetting variability is similar between watersheds, illustrated by high Pearson R values. Interannual variability is least correlated for Horton Index and evapotranspiration as these are controlled by unique watershed landscape features.

	Pearson R					
	ET	**S**	**U**	**W**	**HI**	**NDVI**
CC; RB	0.97	0.95	0.98	1.00	0.93	0.83
CC; EC	0.93	0.92	0.93	0.99	0.84	0.87
CC; PC	0.92	0.93	0.95	0.98	0.83	0.88
CC; MC	0.89	0.91	0.92	0.97	0.84	0.87
CC; BC	0.83	0.89	0.89	0.94	0.76	0.79
CC; LC	0.57	0.84	0.88	0.90	0.55	0.61
RB; EC	0.95	0.96	0.97	1.00	0.93	0.92
RB; PC	0.95	0.94	0.96	0.99	0.92	0.91
RB; MC	0.92	0.91	0.91	0.98	0.80	0.70
RB; BC	0.84	0.85	0.93	0.96	0.81	0.61
RB; LC	0.54	0.85	0.87	0.93	0.64	0.48
EC; PC	0.94	0.94	0.93	0.99	0.88	0.94
EC; MC	0.87	0.90	0.87	0.98	0.71	0.74
EC; BC	0.80	0.83	0.87	0.94	0.68	0.60
EC; LC	0.48	0.80	0.82	0.88	0.45	0.48
PC; MC	0.93	0.91	0.91	0.99	0.74	0.80
PC; BC	0.84	0.86	0.90	0.95	0.65	0.70
PC; LC	0.51	0.84	0.87	0.90	0.49	0.52
MC; BC	0.87	0.86	0.88	0.98	0.74	0.94
MC; LC	0.56	0.85	0.81	0.95	0.41	0.82
BC; LC	0.68	0.85	0.85	0.98	0.50	0.90
minimum	0.48	0.80	0.81	0.88	0.41	0.48
mean	0.80	0.88	0.90	0.96	0.72	0.76
maximum	0.97	0.96	0.98	1.00	0.93	0.94

Table 2.15. Hydrologic Partitioning Trends over Entire Period and Period of Greatest Warming. This table presents the amount of change over time in hydrologic partitioning over the entire period of record and 1964 – 2014, which was chosen because it is the period of the greatest rate of change in annual temperature. Only coefficients with significant ($p<0.05$) trends are presented. Two ** denotes significance at $p<0.001$; One * denotes significance at $p<0.01$; No asterisk denotes significant at $p<0.05$.

	Change Per Decade						
	CC	**RB**	**EC**	**PC**	**MC**	**BC**	**LC**
Annual Evapotranspiration (mm)							
Entire Dataset	NA	NA	NA	NA	NA	NA	-11
1964 - 2014	NA	NA	NA	NA	NA	NA	NA
Annual Stormflow (mm)							
Entire Dataset	NA	NA	NA	NA	NA	NA	NA
1964 - 2014	NA	NA	NA	NA	NA	NA	-12
Annual Baseflow (mm)							
Entire Dataset	NA	NA	NA	NA	NA	NA	NA
1964 - 2014	NA	NA	NA	NA	NA	NA	NA
Annual Wetting (mm)							
Entire Dataset	NA	NA	NA	NA	NA	NA	NA
1964 - 2014	NA	NA	NA	NA	NA	NA	NA
Annual Horton Index							
Entire Dataset	NA	NA	NA	NA	NA	0.007*	-0.007
1964 - 2014	NA	NA	NA	0.021*	0.012	NA	NA

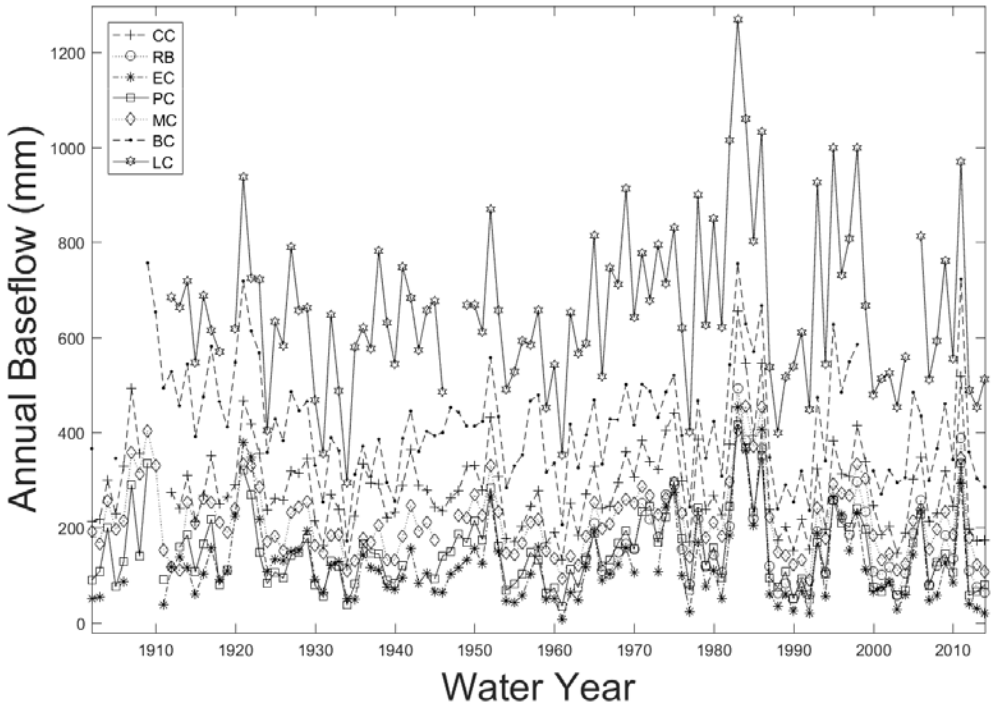

Figure 2.16. Annual Baseflow Time Series. In the seven watersheds, annual baseflow ranges from 7 mm to 1269 mm during 1902 – 2014 with watershed means ranging from 120 mm to 650 mm. There is no significant trend in annual baseflow over time.

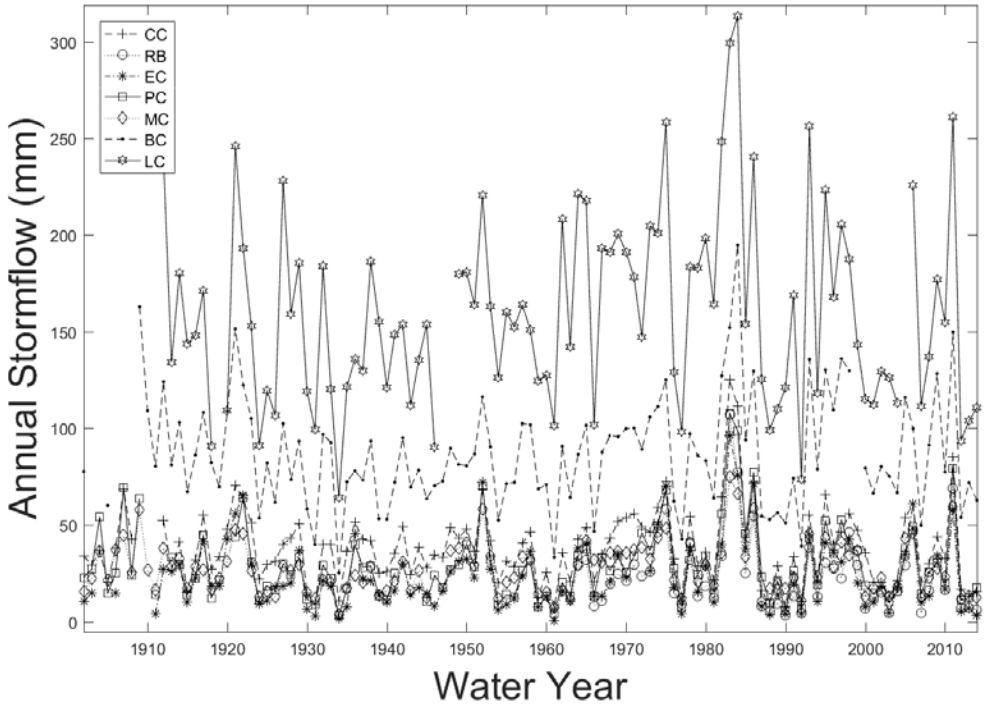

Figure 2.17. Annual Stormflow Time Series. In the seven watersheds, annual stormflow ranges from 0 mm to 313 mm during 1902 – 2014 with watershed means ranging from 20 mm to 160 mm. There is no significant trend in annual stormflow over time, except for a decrease of -12mm / decade in LC that is significant ($p = 0.030$) during the period of greatest warming (1964 – 2014), but not significant during the entire period of record.

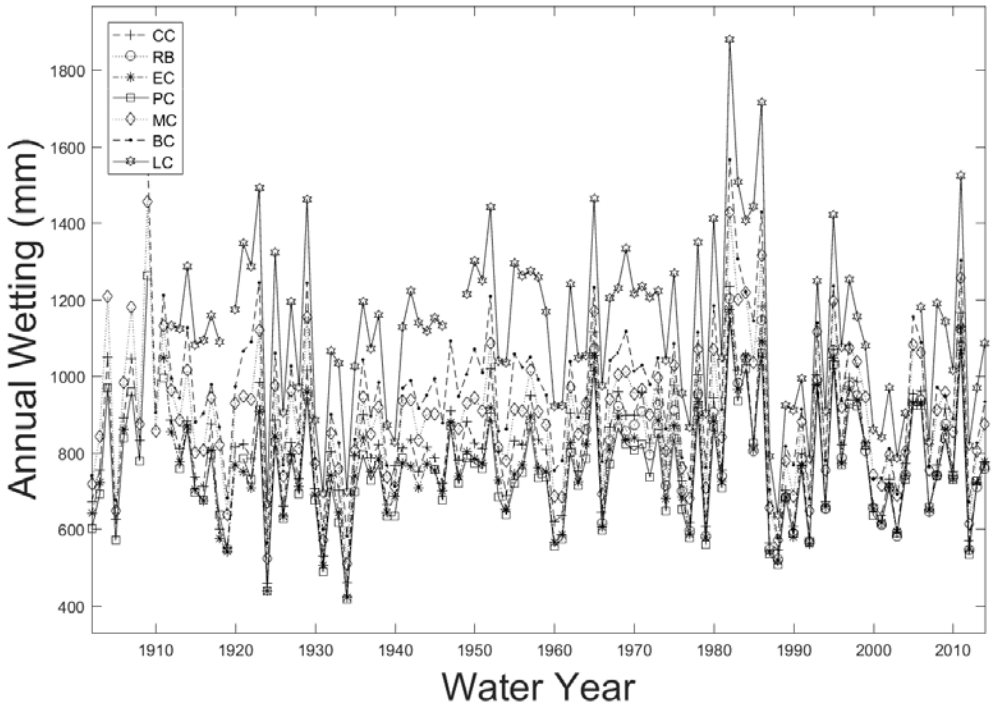

Figure 2.18. Annual Wetting Time Series. In the seven watersheds, annual wetting ranges from 416 mm to 1880 mm during 1902 – 2014 with watershed means ranging from 750 mm to 1120 mm. There is no significant trend in annual wetting over time.

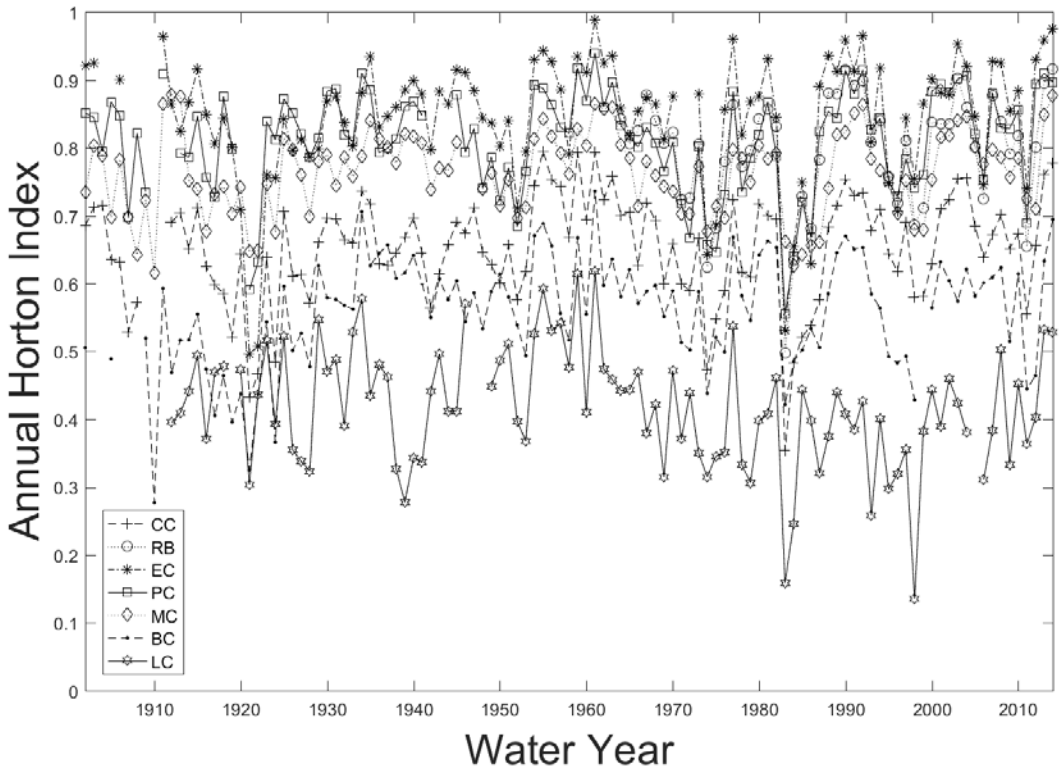

Figure 2.19. Horton Index over Time. Horton Index ranges from 0.14 in LC to 0.99 in EC. There is significant interannual variability in Horton Index within each watershed. No significant trend is present in Horton Index during the period of record.

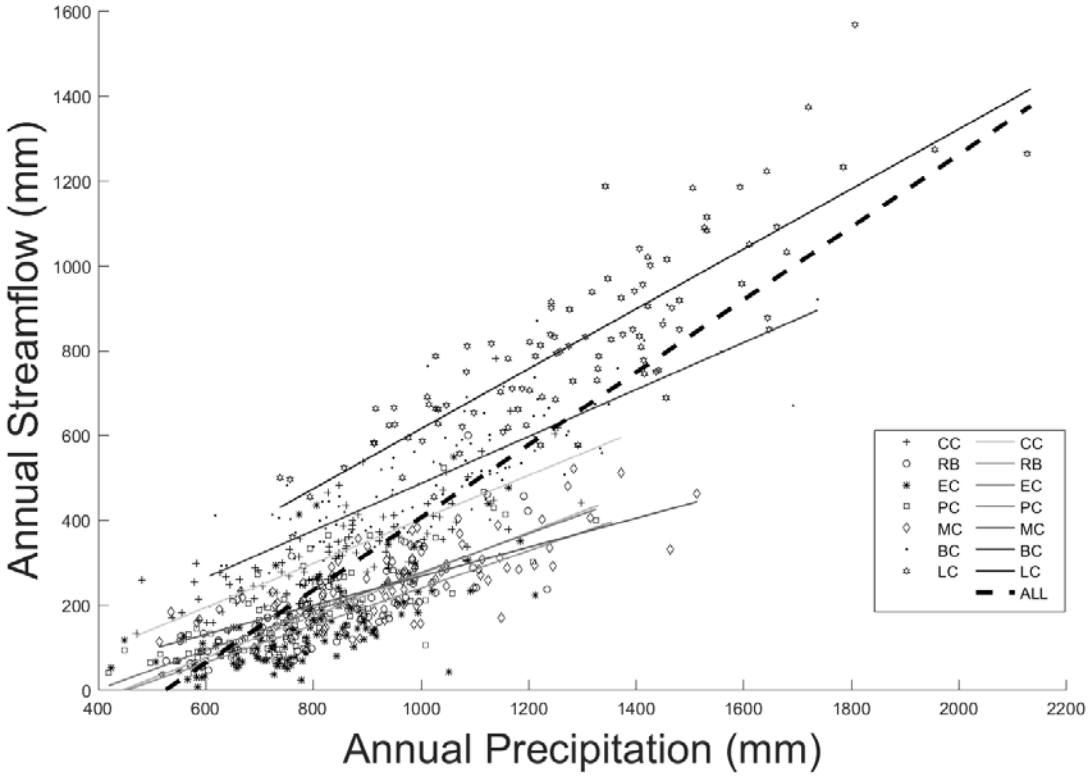

Figure 2.20. Correlation between Precipitation and Streamflow. Annual precipitation correlates well with annual streamflow. Statistical values of the correlations for each watershed are presented in Table 2.16. The black dashed line represents the correlation of precipitation and streamflow for all seven watersheds combined, which would be useful for a broad view analysis. However, it is clear that the points for each watershed are grouped together, rather than randomly scattered around the black dashed line. Correlations between annual streamflow and annual precipitation within individual watersheds illustrates differences in the streamflow and precipitation relationship between the seven watersheds.

Table 2.16: Regression Analysis Statistics for Precipitation and Streamflow. These statistics correspond with the correlations in Figure 2.20. The slope of the line indicates the mm of increase in streamflow for every mm increase in precipitation, or the incremental water yield. The X intercept indicates the amount of precipitation necessary to initiate streamflow. R^2 values between 0.44 – 0.73 indicate that while precipitation accounts for significant streamflow variability, other factors also influence streamflow. Differences in these statistics indicate the variable degree of importance and impact that precipitation has on streamflow variability in each watershed.

	CC	**RB**	**EC**	**PC**	**MC**	**BC**	**LC**	**ALL**
X intercept (mm)	225	446	454	398	218	123	129	526
Slope	0.52	0.49	0.44	0.46	0.34	0.55	0.71	0.85
R^2	0.60	0.60	0.44	0.60	0.54	0.67	0.73	0.72

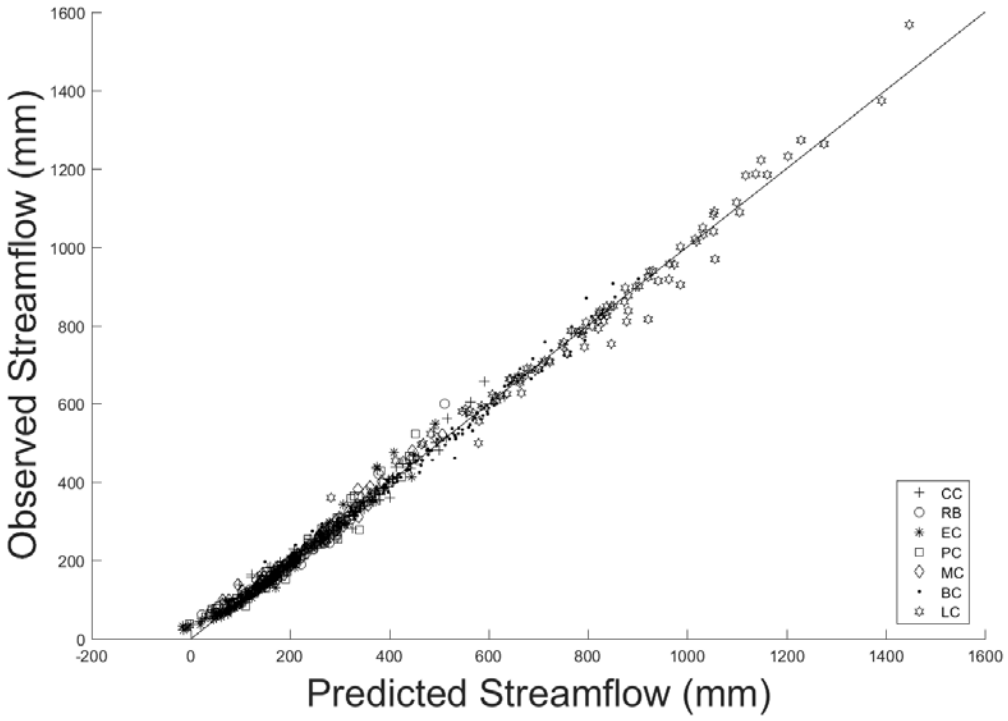

Figure 2.21: Predicted Streamflow Values from Multiple Linear Regression Analysis. The predicted values for streamflow are generated by developing separate equations for each watershed using the coefficients and intercept values for precipitation, winter baseflow, snowmelt rate, snowmelt duration, and snowmelt end date, as shown in Table 2.17. Observed streamflow is predicted for each watershed within 96% accuracy. Predicted and observed streamflow are plotted along with a one to one line that represents a perfect prediction.

Table 2.17: Multiple Linear Regression Analysis of Streamflow Variability. Four metrics in each watershed predict streamflow with less than 4% remaining error, or over 96% accuracy. Figure 2.21 plots the predicted streamflow using the equations provided in this table and the observed values of the metrics used. The degree of influence (coefficient) and predictability added (R^2) of each metric varies by watershed.

	Intercept	Precipitation	Baseflow	Melt Rate	Melt Duration	Melt End Day	Remaining Error
City Creek							
Coefficient	-139	0.036	203	183	0.62		
R^2		0.61	0.17	0.15	0.04		0.02
Red Butte							
Coefficient	-206	-0.048	238	179		0.76	
R^2		0.64	0.15	0.14		0.04	0.03
Emigration							
Coefficient	-73	-0.017	209	179	0.52		
R^2		0.46	0.21	0.25	0.05		0.04
Parleys							
Coefficient	-85	-0.007	239	165	0.56		
R^2		0.59	0.15	0.17	0.05		0.03
Millcreek							
Coefficient	-78	0.019	171	203	0.32		
R^2		0.60	0.22	0.11	0.04		0.03
Big Cottonwood							
Coefficient	-266	0.026	246	148	1.62		
R^2		0.69	0.15	0.10	0.05		0.02
Little Cottonwood							
Coefficient	-519	0.024	273	147	3.27		
R^2		0.73	0.06	0.07	0.11		0.02

Table 2.18. NDVI Mean, Variability, and Trend. The mean covers a range of values throughout the seven watersheds. A significant increase in NDVI exists in three watersheds. However, a significant temperature trend does not exist over a similar period of time. Only coefficients with significant ($p<0.05$) trends are presented. Two ** denotes significance at $p<0.001$; One * denotes significance at $p<0.01$; No asterisk denotes significant at $p<0.05$.

	CC	**RB**	**EC**	**PC**	**MC**	**BC**	**LC**
NDVI							
Mean	0.73	0.79	0.70	0.74	0.78	0.70	0.61
Standard Deviation	0.02	0.02	0.02	0.03	0.02	0.02	0.02
Trend (Change/Decade)							
NDVI (2000 - 2015)	NA	NA	NA	NA	0.018	0.030*	0.029**
Temperature (°C) (2000-2014)	NA	NA	NA	NA	NA	NA	NA

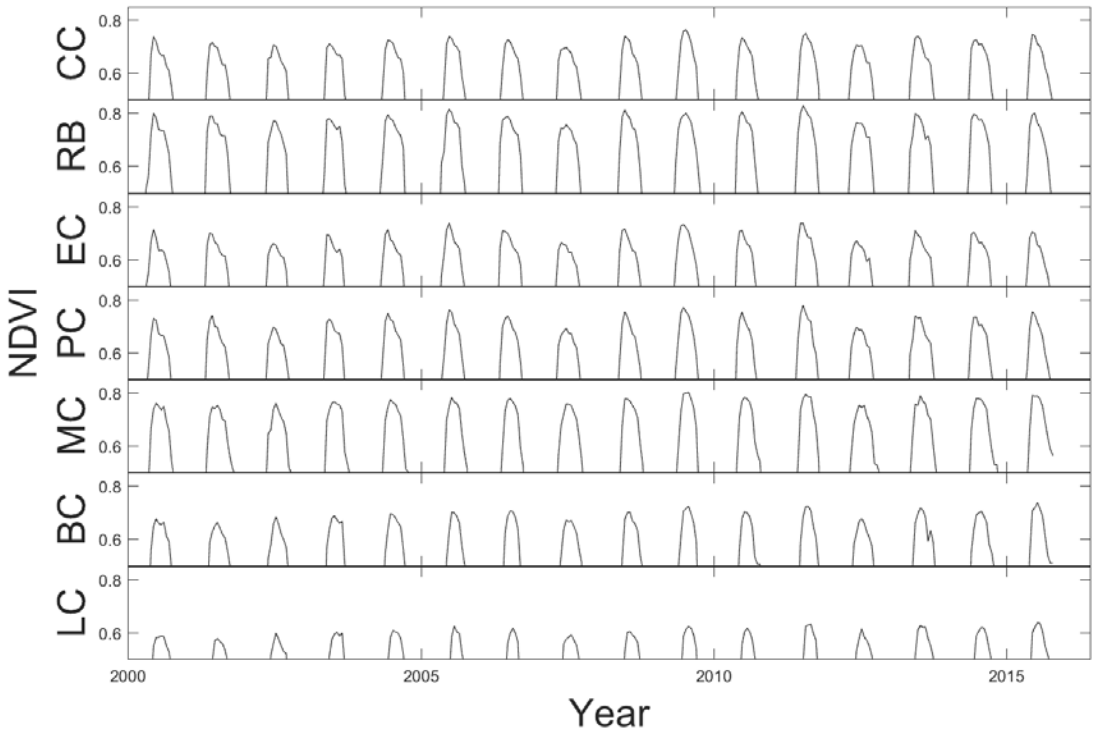

Figure 2.22: NDIV Time Series. NDVI reaches its peak during the growing season. Variation in NDVI within each growing season is less than 0.2 and represents remotely sensed changes in plant greenness. Different watersheds and different years exhibit unique patterns in plant greenness throughout the growing season. Greater variability occurs during the spring and fall when NDVI values represent a mixture of vegetation greenness and snow cover. To highlight changes in the growing season, winter minimum values (often ~0) are not shown.

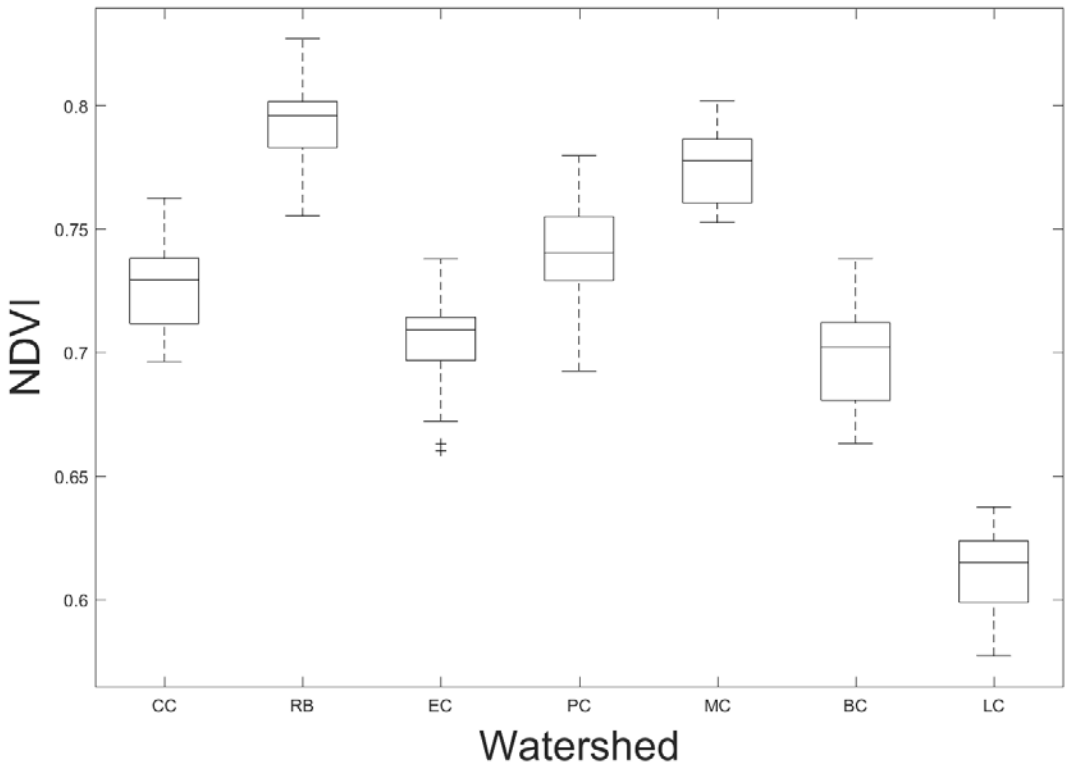

Figure 2.23. Annual Peak NDVI Variability. Peak NDVI ranges from 0.58 in LC to 0.83 in RB. There is significant interannual variability in peak NDVI within each watershed.

Table 2.19: Regression Analysis of NDVI and Winter Baseflow. A positive correlation exists in all watersheds except LC, suggesting that NDVI and winter baseflow likely are supplied through similar processes. However, this relationship is significant ($p < 0.05$) in only CC and RB, suggesting a lack of widespread interconnected between the sources for vegetation and baseflow generation.

	Slope	**P Value**	**R^2**
City Creek	1.97	0.046	0.23
Red Butte	1.73	0.030	0.28
Emigration	0.86	0.163	0.08
Parleys	0.63	0.359	0.00
Millcreek	2.70	0.092	0.15
Big Cottonwood	3.16	0.121	0.12
Little Cottonwood	-0.97	0.664	0.00

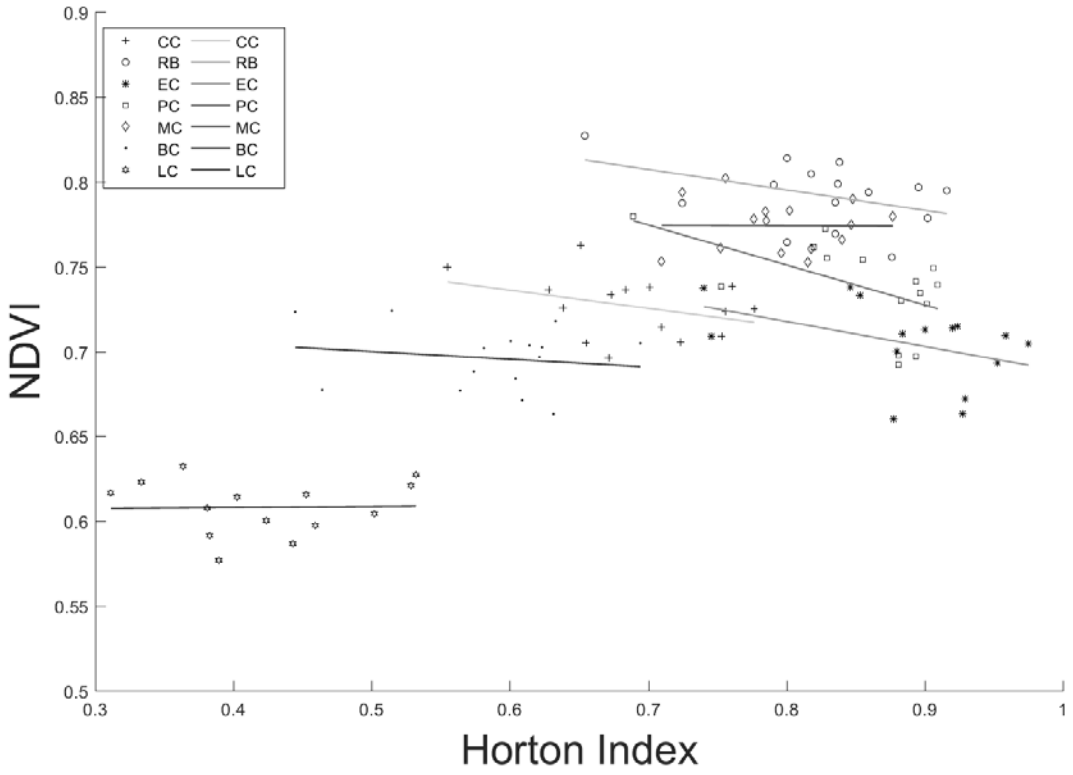

Figure 2.24. NDVI and Horton Index Correlation. In general, vegetation in wetter watersheds (those with lower Horton Index values) show less of a response to drying than in drier watersheds. Significant variability around these trends may be due to the influence of the relative amount of stored water from previous years on vegetation growth. Specific correlation coefficients and goodness of fit for the regression in each watershed is presented in Table 2.20.

Table 2.20: Horton Index and NDVI Correlation. Regression coefficients for the relationships presented in Figure 2.24.

	CC	RB	EC	PC	MC	BC	LC
X intercept	0.80	0.89	0.84	0.94	0.78	0.72	0.61
Coefficient	-0.11	-0.12	-0.15	-0.24	-0.003	-0.045	0.006
R^2	0.057	0.12	0.12	0.26	0.00	0.00	0.00
P value	0.20	0.11	0.12	0.03	0.97	0.57	0.93